iScience

CellPress
OPEN ACCESS

Article

TWIK-related acid-sensitive K^+ channel 2 promotes renal fibrosis by inducing cell-cycle arrest

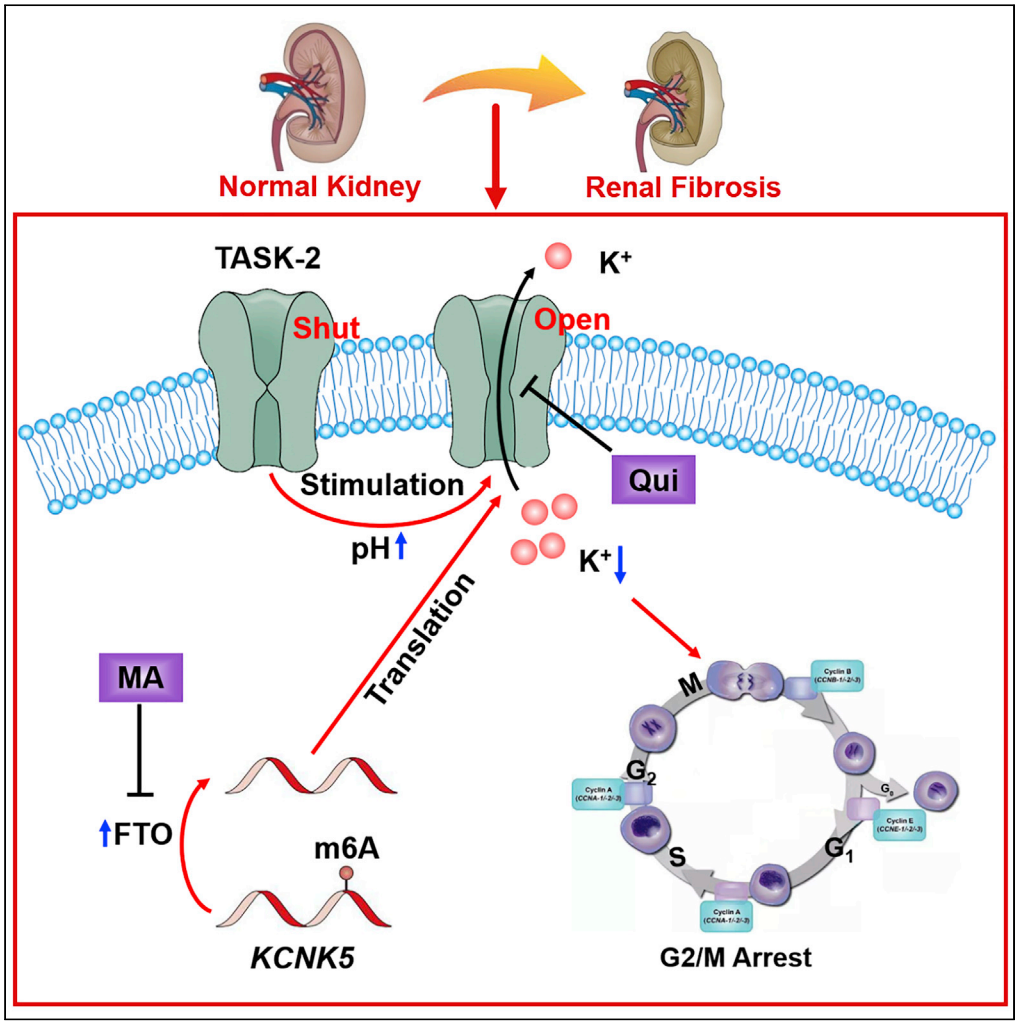

Jian Zhang, Jing Chen, Yufei Lu, ..., Zhichao Liu, Nana Song, Xiaoqiang Ding

song.nana@zs-hospital.sh.cn (N.S.)
ding.xiaoqiang@zs-hospital.sh.cn (X.D.)

Highlights

TWIK-related acid-sensitive K^+ channel 2 (TASK-2) is up-regulated in renal fibrosis

Inhibition of TASK-2 alleviates renal fibrosis via reducing G2/M arrest

Activation of TASK-2 reduced intracellular K^+ and leads to fibrogenesis

TASK-2 overexpression in renal fibrosis is mediated by FTO through m6A modification

Zhang et al., iScience 25, 105620
December 22, 2022
https://doi.org/10.1016/j.isci.2022.105620

iScience

CellPress
OPEN ACCESS

Article

TWIK-related acid-sensitive K^+ channel 2 promotes renal fibrosis by inducing cell-cycle arrest

Jian Zhang,[1,2,10] Jing Chen,[2,3,4,5,6,10] Yufei Lu,[2,3,4,5,6,10] Yan Yang,[2,3,4,5,6] Weize Chen,[2,3,4,5,6] Bo Shen,[2,3,4,5,6] Jiachang Hu,[2,3,4,5,6] Ping Jia,[2,3,4,5,6] Sujuan Xu,[2,3,4,5,6] Yiqin Shi,[2,3,4,5,6] Yichun Ning,[2,3,4,5,6] Jialin Wang,[2,3,4,5,6] Yi Fang,[2,3,4,5,6] Shuan Zhao,[2,3,4,5,6] Yang Li,[2,3,4,5,6] Yan Dai,[2,3,4,5,6] Xiaoyan Zhang,[2,3,4,5,6] Meng Xiang,[7] Yang Tian,[8] Zhichao Liu,[8] Nana Song,[2,3,4,5,6,9,*] and Xiaoqiang Ding[2,3,4,5,6,11,*]

SUMMARY

TWIK-related acid-sensitive K^+ channel-2 (TASK-2, encoded by *Kcnk5*) is essential in cell biological processes, by regulating transmembrane K^+ balance. In the present study, we aimed to clarify the role of TASK-2 in renal fibrosis and explore the underlying mechanism. We found that TASK-2 level was elevated in the renal tubular UUO- and UIR-induced renal fibrosis as well as in patients with renal tubulointerstitial fibrosis. Knockout of *Kcnk5* or inhibition of TASK-2 in renal tubules attenuated G2/M cell-cycle arrest and alleviated renal fibrosis. Mechanistically, demethylase fat mass and obesity-associated protein (FTO) reduced N6-adenosine methylation (m6A) of *Kcnk5* mRNA following renal fibrosis. FTO deficiency attenuated the upregulation of TASK-2 and renal fibrosis. The results demonstrated the crucial role of TASK-2 in renal fibrosis, which is conducive to a better understanding of the pathogenesis of renal fibrosis. TASK-2 may be a potential treatment strategy to alleviate the development of renal fibrosis.

INTRODUCTION

Renal fibrosis is the final common outcome of chronic kidney disease (CKD) irrespective of the underlying etiology.[1] CKD is a highly life-threatening public health issue worldwide; however, the exact pathogenesis of renal fibrosis remains to be elucidated. The pathophysiological mechanism of renal fibrosis is complex, involving interstitial inflammation, tubular apoptosis, myofibroblast proliferation, and progressive accumulation of extracellular matrix, ultimately leading to fibrotic lesions and tissue scarring.[2] A consequence of fibrotic injury is cell-cycle arrest in the G2 phase in tubular epithelial cells.[3] Numerous signals and molecular mediators are involved in the development of renal fibrosis, with multiple lines of evidence indicating imbalances in potassium level as influencing the course of kidney diseases. Low dietary potassium intake increases the risk of CKD development and progression of kidney disease, whereas increasing potassium intake can prevent kidney damage.[4–6] Previous studies report that a high-potassium diet is renoprotective in cyclosporine-induced nephrotoxicity,[7] and that potassium supplementation can reduce renal inflammation and injury in subtotal nephrectomy rats, independent of a blood-pressure-regulatory mechanism.[8] However, the mechanism underlying the renoprotective effect of potassium remains elusive.

Intracellular K^+ is essential for cell proliferation,[9] and K^+ efflux results in cell shrinkage (decreased apoptotic volume) and enhances apoptosis.[10] Additionally, cytosolic K^+ directly inhibits the activation of caspases and limits cell proliferation,[11] and activation of K^+ channels is required for cell cycle progression.[12] Accumulating evidence indicates that intra- and extracellular K^+ imbalance contributes to fibrotic progression. Potassium channels underlie the K^+-permeability of the cell membrane, and a Ca^{2+}-activated K^+ channel (KCa3.1) specifically promotes renal fibrosis,[13] as KCa3.1 blockade ameliorates renal interstitial fibrosis in diabetic nephropathy and unilateral ureteral obstruction (UUO) mice.[14,15] In the large family of K^+ channels, TWIK-related acid-sensitive K^+ channel-2 (TASK-2; a two-pore-domain K^+ channel) is highly expressed in renal tubules.[16] TASK-2 generates background K^+ currents that are increased by external and internal alkalization and regulates the cell volume of renal proximal tubule cells.[17] TASK-2 adapts K^+ conductance

[1]Institutes of Biomedical Sciences, Fudan University, Shanghai 200032, China

[2]Department of Nephrology, Zhongshan Hospital, Fudan University, Shanghai 200032, China

[3]Shanghai Medical Center of Kidney, Shanghai 200032, China

[4]Shanghai Institute of Kidney and Dialysis, Shanghai 200032, China

[5]Shanghai Key Laboratory of Kidney and Blood Purification, Shanghai 200032, China

[6]Hemodialysis Quality Control Center of Shanghai, Shanghai 200032, China

[7]Department of Physiology and Pathophysiology, Fudan University, Shanghai 200032, China

[8]Department of Chemistry, East China Normal University, Shanghai 200241, China

[9]Fudan Zhangjiang Institute, Shanghai 201203, China

[10]These authors contributed equally

[11]Lead contact

*Correspondence: song.nana@zs-hospital.sh.cn (N.S.), ding.xiaoqiang@zs-hospital.sh.cn (X.D.)

https://doi.org/10.1016/j.isci.2022.105620

to the HCO_3^--transport activity in renal tubules, and knockout of the TASK-2 gene (*Kcnk5*) in mice induces metabolic acidosis caused by renal loss of HCO_3^- [16]. These findings suggest that TASK-2 might play an important role in renal epithelia function; however, the role of TASK-2 in the progression of renal fibrosis remains unclear.

In the present study, we found that expression of TASK-2 may be regulated by the posttranscriptional mechanism. N^6-methyladenosine (m^6A) is the most prevalent base modification in mRNA and affects multiple aspects of the mRNA life cycle, including splicing, export, stability, and translation.[18] Thus, m^6A modification is involved in various biological processes. m^6A is a reversible modification, which can be catalyzed by methyltransferases, such as methyltransferase-like (METTL)3 and METTL14, and demethylases, such as Fat mass and obesity-associated protein (FTO).[19] A previous study reported significant elevations in m^6A levels in cisplatin-induced renal injury and that inhibiting FTO mediated m^6A abrogation in RNA and promoted injury.[20] However, in colistin-induced renal injury, METTL3 overexpression played a protective role against oxidative stress and apoptosis,[21] and another study showed that METTL14 promotes renal IRI.[22] Additionally, *FTO* polymorphisms enhance the risk of end-stage renal disease (ESRD).[23] Moreover, m^6A aggravates obstructive nephropathy-induced renal fibrosis.[24] Furthermore, in the UUO kidney, m^6A, METTL3, and METTL14 levels are significantly decreased, and FTO level is increased, whereas *Fto* deficiency attenuates UUO-induced fibrogenic responses in the kidney.[25,26] Therefore, m^6A modification is involved in renal interstitial fibrosis and might be a promising therapeutic target, however, whether the methylation modification of the *Kcnk5* is involved in the progression of renal fibrosis has not been elucidated.

In this study, we investigated the roles of TASK-2 and m^6A modification of its mRNA in renal fibrosis. The data showed that TASK-2 is overexpressed in renal tubules of UUO-and UIR-kidneys and patients with tubulointerstitial fibrosis, and that *Kcnk5* knockdown in renal epithelial cells reduced G2/M cell-cycle arrest and renal fibrosis *in vivo* and *in vitro*. Additionally, we confirmed the co-localization of FTO and TASK-2 in kidney tubules, resulting in TASK-2 demethylation following renal injury.

RESULTS

TWIK-related acid-sensitive K^+ channel-2 level is elevated in renal tubules of mice with unilateral ureteral obstruction - and unilateral ischemia reperfusion-induced fibrosis and patients with tubulointerstitial fibrosis

Potassium channels are important in the fibrogenic progress. Here, we examined TASK-2 expression in the UUO- and UIR-kidney. Immunofluorescence results showed that TASK-2 is mainly expressed in proximal tubule epithelial cells (AQP-1 positive) and distal tubule epithelial cells (NCC positive) with the highest abundance in proximal tubule epithelial cells, however, is rarely localized in Henle's loop (THP positive) or collecting tubes (AQP-2 positive) (Figure 1A). Additionally, we found elevated TASK-2 expression in renal tubules of UUO and UIR mice. Renal fibrosis was confirmed via reduced E-cadherin and elevated fibronectin 1 (FN-1) and α-SMA levels (Figures S1A and S1B). Western blot results verified significantly elevated TASK-2 levels (Figures 1B and 1C), whereas *Kcnk5* mRNA levels weren't significantly changed in kidneys of UUO and UIR mice (Figures 1D and 1E), suggesting that the posttranscriptional regulation of *Kcnk5* might be involved in renal fibrosis. Moreover, it was further proved that the up-regulation of TASK-2 in proximal tubules (LTL positive) of patients with renal tubulointerstitial fibrosis was in line with the extent of fibrosis demonstrated by Masson staining (Figure 1F).

Kcnk5 knockout in kidney epithelium alleviates renal fibrosis in unilateral ureteral obstruction and UIR mice

To investigate the role of TASK-2 in renal fibrosis, we generated conditional renal tubular *Kcnk5*-knockout mice ($Kcnk5^{fl/fl}/Cdh16^{cre}$) by crossing $Kcnk5^{fl/fl}$ mice with *Cdh16*-Cre mice (Figure S2A), followed by the assessment of the role of TASK-2 in these mouse models of UUO- and UIR-induced renal fibrosis. After the confirmation of the $Kcnk5^{fl/fl}$ or wild-type allele and the *Cdh16*-Cre transgene by PCR (Figure S2B), we verified TASK-2 deficiency in the proximal tubular by immunohistochemistry and immunofluorescence double staining (Figures S2C and S2D). We found that elevated TASK-2 level in proximal tubulars of the UUO and UIR kidney was inhibited in $Kcnk5^{fl/fl}/Cdh16^{cre}$ mice (Figures S2E and S2F).

Moreover, the evaluation of fibrotic severity in kidney from WT, $Kcnk5^{fl/fl}$, and $Kcnk5^{fl/fl}/Cdh16^{cre}$ mice by Masson's trichrome staining at 14 days after UUO and UIR onset revealed attenuated collagen accumulation

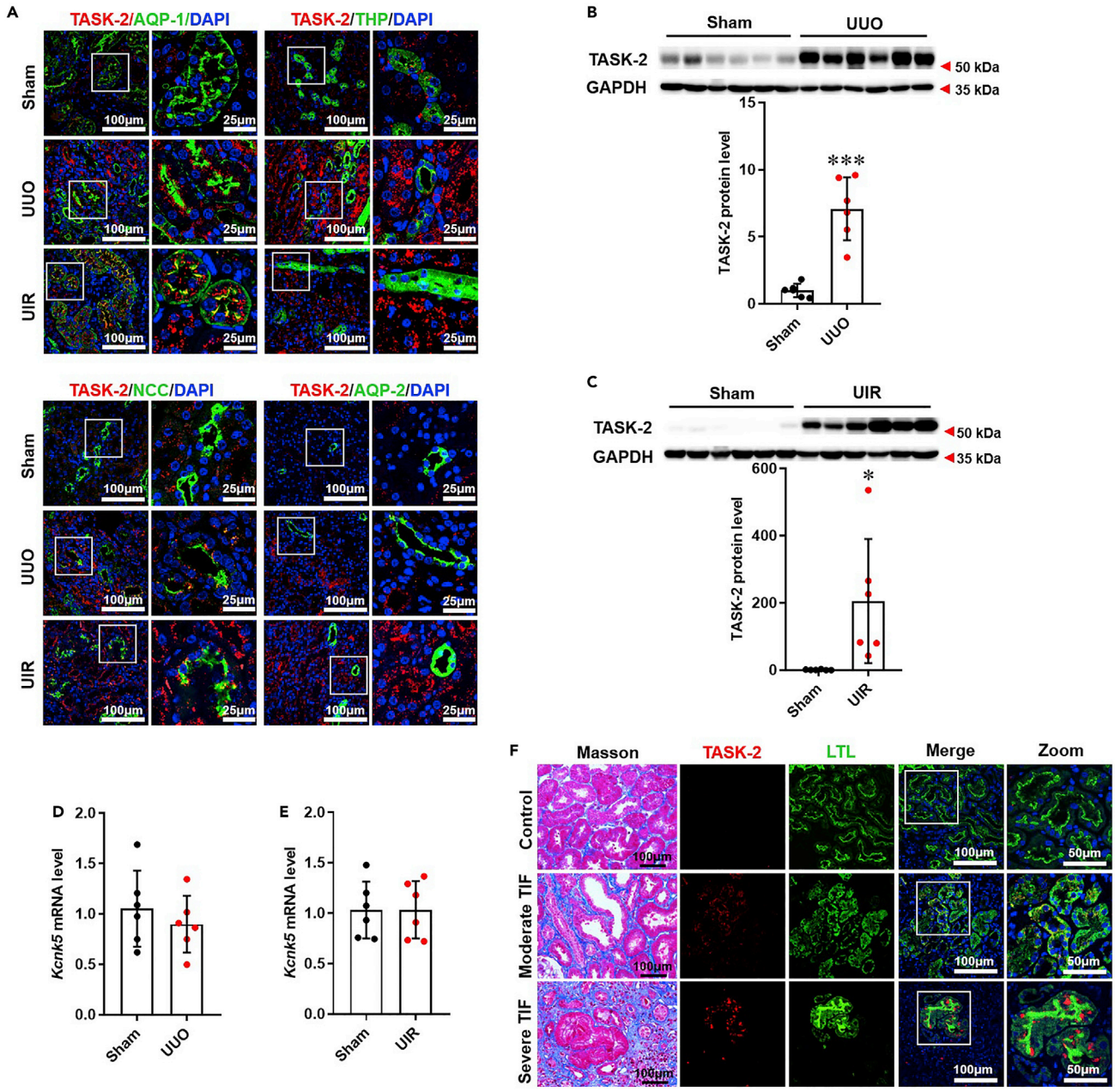

Figure 1. Upregulation of TASK-2 in renal fibrosis

(A) TASK-2 co-localization according to immunostaining for AQP1, THP, NCC, and AQP2 in Sham, UUO and UIR kidneys (scale bar 100 μm, zoom 25 μm).

(B and C) Representative western blot of TASK-2 expression in Sham, UUO, and UIR kidneys. Elevated TASK-2 expression in UUO (n = 6) (B) and UIR (n = 6) (C) kidneys.

(D and E) Real-time qPCR analysis of *Kcnk5* mRNA levels in Sham, UUO (n = 6) (D), and UIR (n = 6) (E) kidneys.

(F) Representative images of Masson's trichrome staining (scale bar 100 μm), and TASK-2 co-localization with LTL in human kidneys with tubulointerstitial fibrosis (TIF) (scale bar 100 μm, zoom 50 μm). Data represent the mean ± SD. A two-tailed, unpaired t test (B–E) was used to determine statistical significance. *p < 0.05, **p < 0.01, ***p < 0.001.

(blue staining) in kidneys of *Kcnk5*$^{fl/fl}$/*Cdh16*^{cre} mice (Figure 2A), with immunofluorescence staining of α-SMA in UUO and UIR kidneys from mice with the three genotypes confirming this pattern (Figure 2B). Furthermore, western blot analysis of kidneys from WT and *Kcnk5*$^{fl/fl}$ mice showed elevations in FN-1 and α-SMA and attenuated E-cadherin levels relative to Sham controls, whereas FN-1 and α-SMA levels were significantly lower and E-cadherin were higher in UUO and UIR kidneys from the *Kcnk5*$^{fl/fl}$/*Cdh16*^{cre} cohort

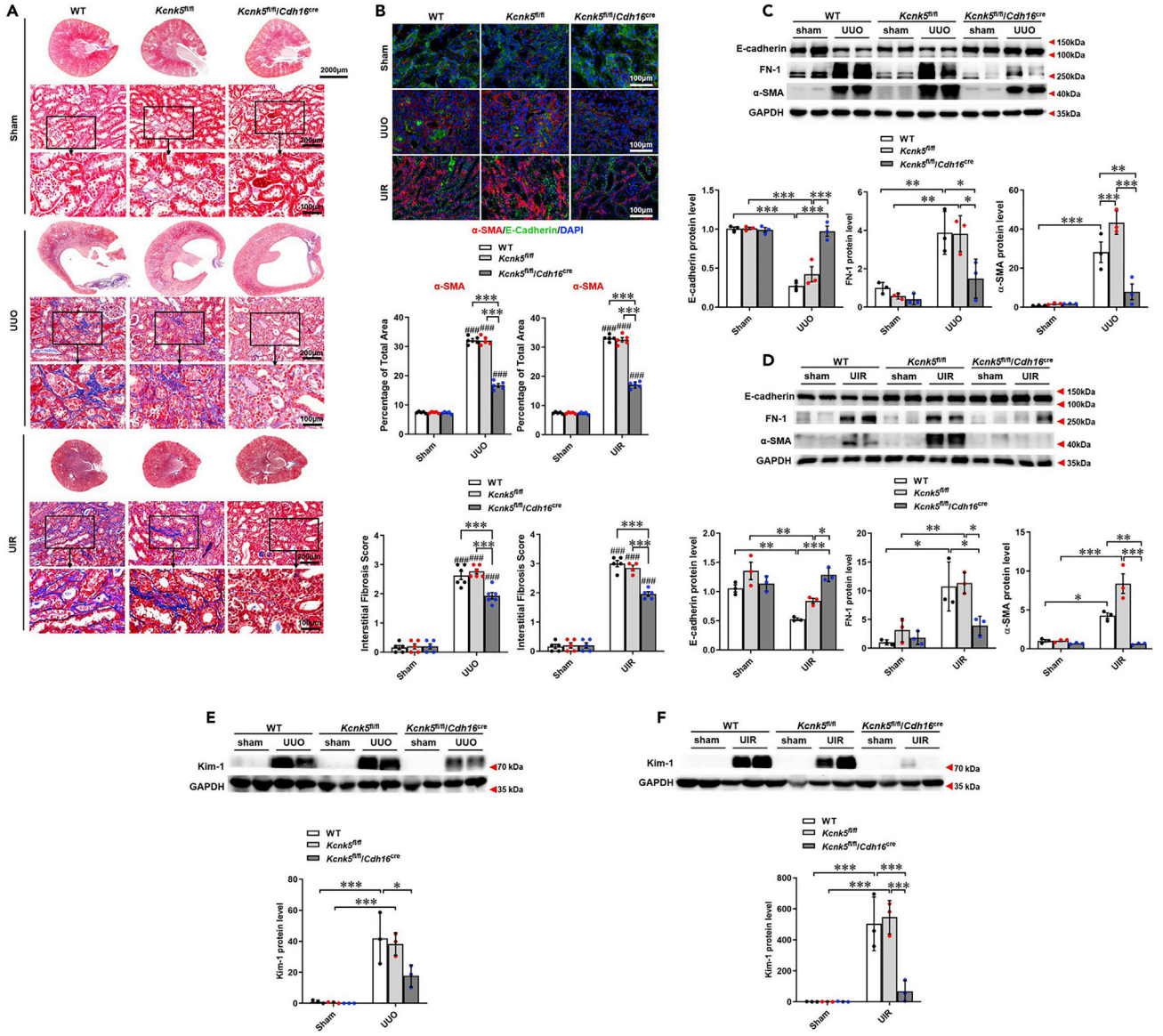

Figure 2. *Kcnk5* knockout attenuates kidney fibrosis

Assessment of the degree of tubulointerstitial fibrosis in WT, *Kcnk5*$^{fl/fl}$, and *Kcnk5*$^{fl/fl}$/*Cdh16*^{cre} mice 14 days after Sham, UUO, and UIR surgery.

(A) Representative images of Masson's trichrome staining (scale bar 2000 μm, zoom 200 μm, 100 μm); n = 5 in Sham and UIR groups, n = 6 in UUO group.

(B) Immunostaining for α-SMA and E-cadherin (scale bar 100 μm); n = 5.

(C and D) Western blot analysis of E-cadherin, FN-1, and α-SMA expression in UUO (C) and UIR (D) kidneys.

(E and F) Western blot analysis of Kim-1 expression in UUO (E) and UIR (F) kidneys. *p < 0.05, **p < 0.01, ***p < 0.001, ###p < 0.001 (vs. the Sham group) by two-way ANOVA, mean ± SD.

(Figures 2C and 2D). Because fibrosis often follows the initial kidney injury, therefore Kidney injury molecule 1 (Kim-1) was evaluated. The results showed that Kim-1 was elevated in UUO and UIR kidneys, and ablated after *Kcnk5* knockout (Figures 2E and 2F).

Knockout of TASK-2 in the kidney epithelium alleviated G2/M arrest of renal tubular epithelial cells in unilateral ureteral obstruction and UIR mice

G2/M-arrested proximal tubular cells are considered a major source of profibrotic cytokine production.[27] To analyze the effect of TASK-2 on the cell cycle distribution of proximal tubular epithelial cells *in vivo*, we conducted immunofluorescence staining of cell cycle markers by labeling proliferating cells (G1, S, G2 and

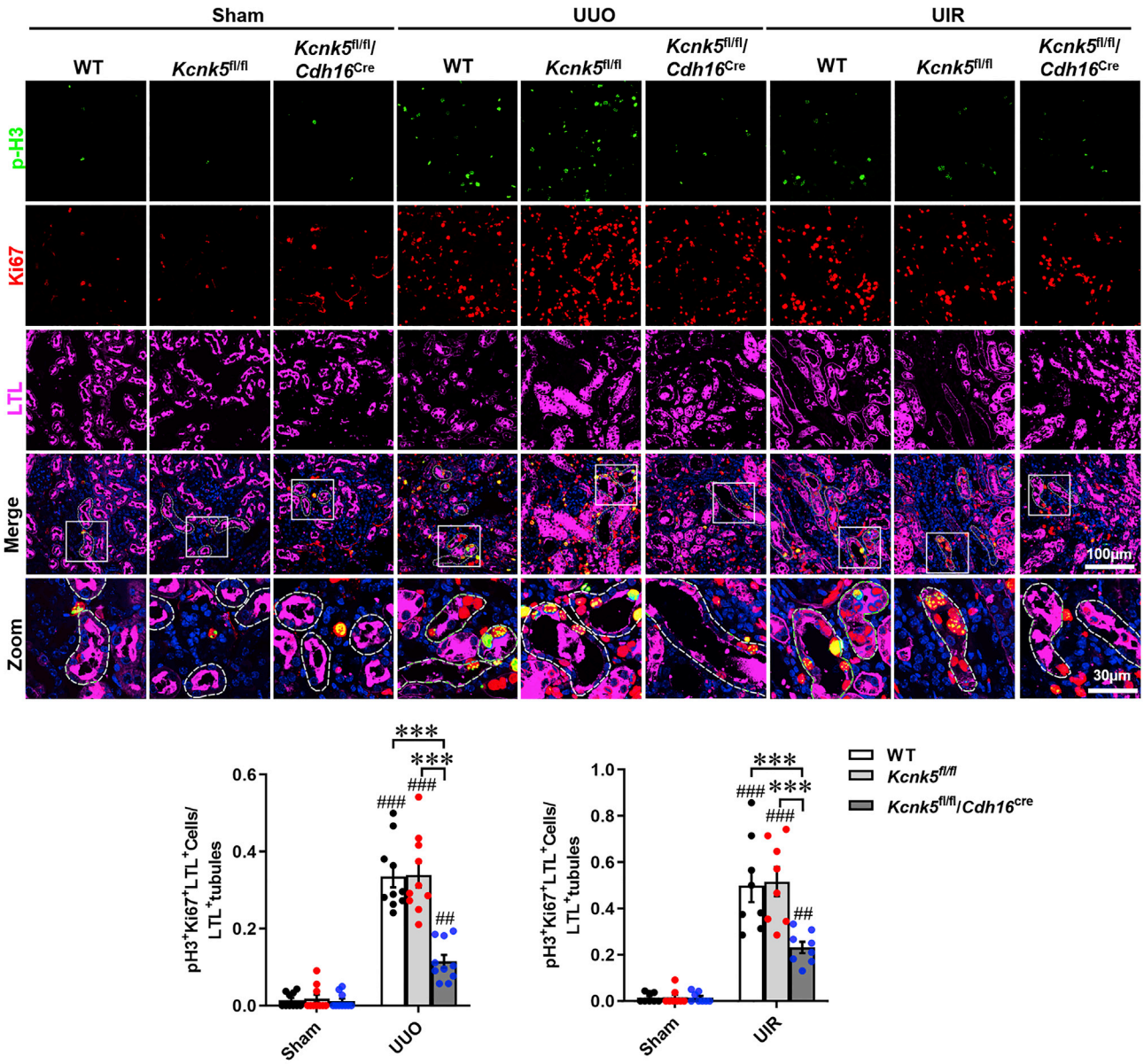

Figure 3. *Kcnk5* knockout reduces G2/M cell-cycle arrest in UUO and UIR mice

Co-immunostaining for pH3 and Ki67 in sham, UUO, and UIR kidneys. (scale bar 100 μm, zoom 30 μm). Counting of $pH3^+Ki67^+LTL^+$ cells in LTL^+ tubules (n = 5 × 2 in Sham and UUO groups, n = 4 × 2 in UIR group). ***$p < 0.001$, $^{###}p < 0.001$ (vs. the Sham group) by two-way ANOVA, mean ± SD.

M phase) with Ki67 specific antibody and detecting those in G2/M phase by staining with the phosphorylation of histone H3 at Ser10 (pH3) followed by the staining of LTL. The number of G2/M phase cells ($pH3^+$ and $Ki67^+$) in LTL-positive tubules was calculated. The results indicated that a few proliferating cells were localized in the renal interstitium of Sham mice. However, an accumulation of proliferating renal tubular epithelial cells in the G2/M phase was detected in UUO and UIR kidneys of WT and *Kcnk5*$^{fl/fl}$ mice, whereas fewer cells in this phase were found in *Kcnk5*$^{fl/fl}$/*Cdh16*^{cre} mice relative to WT and *Kcnk5*$^{fl/fl}$ mice (Figure 3).

TWIK-related acid-sensitive K^+ channel-2 is upregulated in TGF-β-induced fibrotic changes in HK-2 cells *in vitro*

We then investigated the detailed profibrotic mechanisms of TASK-2 in TGF-β1 induced fibrotic changes of HK-2 cells. We assessed tubular transdifferentiation by immunoblotting for E-cadherin, FN-1, and α-SMA in

HK-2 cells after exposure to various doses of TGF-β1 (2, 5, 10, 15 ng/mL) (Figure S3A). The results showed that TGF-β1 treatment (10 ng/mL) for 24 h decreased E-cadherin and increased FN-1 and α-SMA levels (Figures S3B and S3C), with TGF-β1-induced fibrotic changes confirmed by morphological alterations from an epithelial to a typical spindle-like fibroblastic shape (Figure S3D). Additionally, TGF-β1 promoted HK-2 cell migration and proliferation according to wound-healing assays and CCK-8 detection (Figures S3E and S3F). Consistent with findings observed *in vivo*, treatment with TGF-β1 elevated TASK-2 level, but reduced *KCNK5* mRNA level (Figures S3G and S3H).

TWIK-related acid-sensitive K^+ channel-2 activity is upregulated during fibrotic changes in HK-2 cells *in vitro*

TASK-2 is a pH-sensitive K^+ channel, and both intracellular and extracellular alkalization can stimulate TASK-2 activity to promote an outward K^+ current. To investigate whether upregulated TASK-2 expression affects its activity during fibrogenic progression, we measured intracellular and extracellular pH and intracellular K^+ levels (Figures S4A, S4B, and 4A–4D). We found that TGF-β treatment decreased extracellular pH from 7.45 ± 0.006 to 7.34 ± 0.015 and intracellular K^+ from 142.8 ± 8.4 mM to 108.6 ± 14.7 mM, but increased intracellular pH from 7.16 ± 0.02 to 7.86 ± 0.07 (Figures 4A and 4B). Notably, intracellular K^+ was restored by blocking TASK-2 with quinidine or with si*KNCK5* during TGF-β induced fibrotic changes in HK-2 cells (Figures 4C and 4D). To further determine the role of TASK-2 on the fibrotic changes of HK-2 cells, we added 30 mM $NaHCO_3$ to alkalize extracellular medium from 7.45 ± 0.006 to 7.87 ± 0.06 and confirmed that pretreatment with $NaHCO_3$ increased intracellular pH from 7.16 ± 0.02 to 7.48 ± 0.10 and decreased intracellular K^+ concentration (from 142.8 ± 8.4 mM to 115.1 ± 11.8 mM). Additionally, alkaline conditions (pH 7.8) exacerbated TGF-β-induced low intracellular K^+ (88.9 ± 7.8 mM) and fibrotic changes, according to observed increased α-SMA and FN-1, and reduced E-cadherin expression (Figures 4E–4I). These data suggested that TGF-β-induced intracellular alkalization stimulated TASK-2 to promote upregulated K^+ efflux.

TWIK-related acid-sensitive K^+ channel-2 inhibition attenuates TGF-β-induced fibrotic changes *in vitro*

To determine the roles of TASK-2 in renal fibrosis *in vitro*, we evaluated the effects of quinidine (a TASK-2 inhibitor) and *KCNK5* silencing on TGF-β-stimulated fibrotic changes in HK-2 cells. HK-2 cells were pretreated with different concentrations of quinidine (20, 40, 60, 80, 100 μM) before treatment with TGF-β1 (10 ng/mL) for 24 h. The fibrotic changes of HK-2 were evaluated according to E-cadherin, FN-1, and α-SMA levels. The results showed that 80 μM quinidine significantly inhibited TGF-β1-induced fibrotic changes of HK-2 cells according to reduced α-SMA and FN-1, and upregulated E-cadherin expression without influencing cell viability (Figures S5A–5C and 5A). Additionally, TASK-2 inhibition reduced TGF-β1-induced proliferation and migration of HK-2 cells according to CCK8 assays and wound healing (Figures S5D and S5E). Because quinidine is not a selective inhibitor of TASK-2, we confirmed these findings using another TASK-2 blocker, clofilium (Figure S5F), and *KCNK5* siRNA which effectively knocked down TASK-2 level (Figures S5G–S5I and 5B) These results confirmed that TASK-2 inhibition or knockdown attenuated TGF-β-induced fibrotic changes *in vitro*. Overexpression of TASK-2 in HK-2 cells promoted TGF-β-induced fibrogenesis, furtherly proving the profibrogenic role of TASK-2 (Figures 5C and 5D).

TWIK-related acid-sensitive K^+ channel-2 inhibition suppresses G2/M cell-cycle arrest in TGF-β-treated HK-2 cells

To verify the role of TASK-2 in cell-cycle arrest, we performed immunostaining of Ki67 and pH3 in HK-2 cells and quantified the proportion of cells in the G2/M phase (pH3 positive) among total proliferating cells ($Ki67^+$) (Figure 6A). Additionally, we performed cell cycle analysis by PI staining and flow cytometry (Figures 6B and 6C). In HK-2 cells, TGF-β treatment for 24 h resulted in a marked increase in the percentage of cells in the G2/M phase, whereas pharmacological blocking or deficiency of TASK-2 eliminated this effect.

Reduction of m^6A incorporation in *Kcnk5* mRNA was reduced in renal fibrosis *in vivo*

The opposing changes in TASK-2 protein and *Kcnk5* mRNA levels suggested the involvement of post-transcriptional regulation. m^6A incorporation is the most prevalent method of posttranscriptional regulation,[28] and our study indicated that m^6A modification is essential in the progression of UUO-induced fibrosis (Figure S6A). Thus, we applied MeRIP-seq to explore m^6A modification of mRNA in the UUO

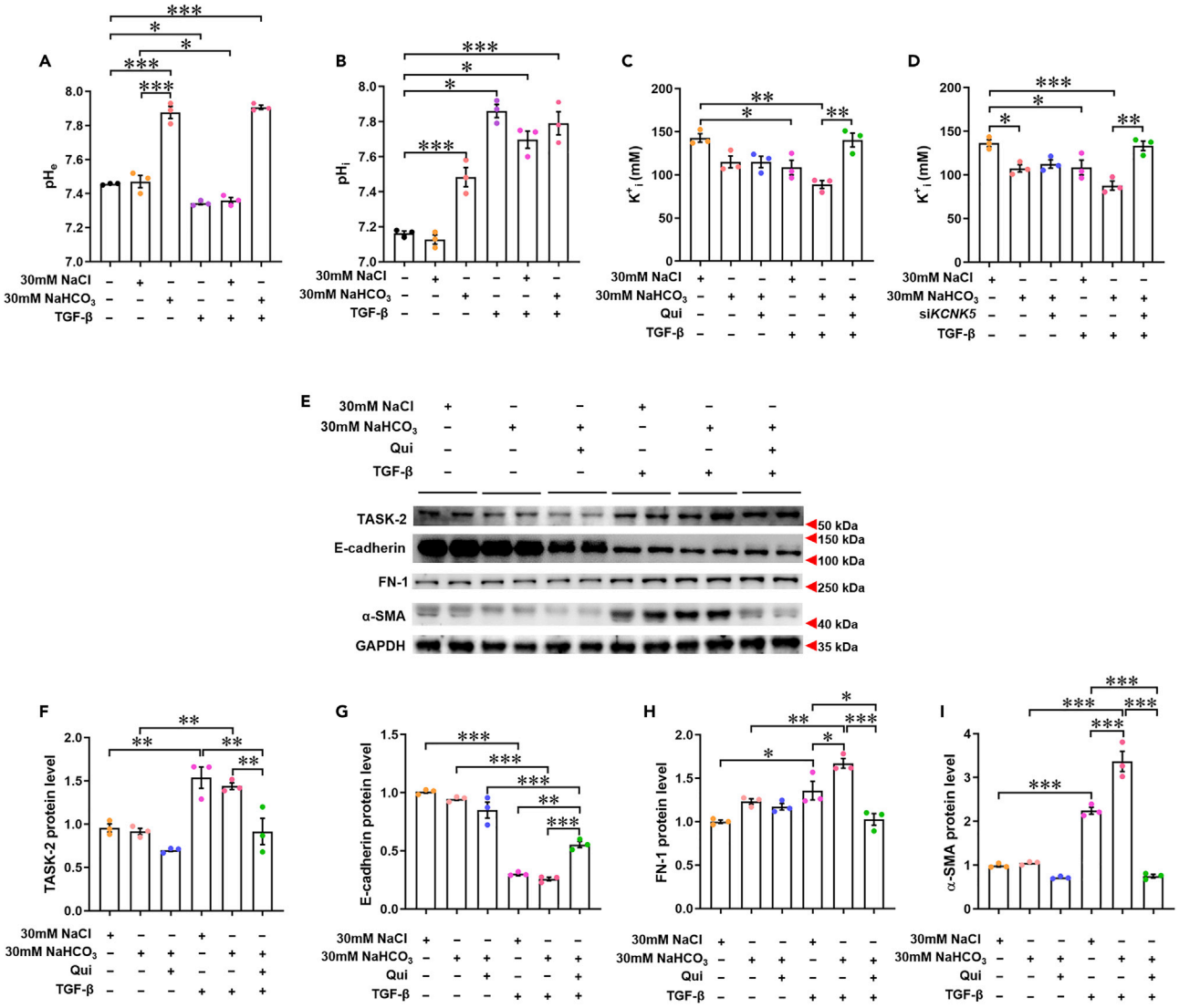

Figure 4. TGF-β treatment promotes TASK-2 activity in HK-2 cells during fibrogenesis

(A) Extracellular pH was measured using a pH meter (n = 3).

(B–D) intracellular pH (B) and K^+ (C and D) levels (n = 3) were determined by flow cytometry after staining with pH-sensitive nanoparticles (CDs@FITC) and K^+-sensitive nanoparticles (AuNPs@aptamer), respectively.

(E–I) Western blot analysis of E-cadherin, α-SMA, FN-1, and TASK-2 expression. *p < 0.05, **p < 0.01, ***p < 0.001 by One-way ANOVA, mean ± SD.

kidneys. We found that m^6A of *Kcnk5* at the 1460th adenosine was significantly reduced in the UUO kidneys (Figure 7A). To clarify which enzyme catalyzes the methylation of *Kcnk5* mRNA, we assessed the expression of demethylases, such as FTO and ALBKH-5, and methyltransferases, such as METTL15, METTL3, METTL14, METTL17, and METTL5. The results showed increased FTO, METTL3 and METTL14 and decreased ALBKH-5, and METTL15 expression in the UUO kidneys (Figure 7B). Among them, increases in the demethylase FTO and decreases in the methyltransferase METTL15 might explain the observed reduction in the m^6A modification of *Kcnk5*. Because METTL15 catalyzes 5-methylcytidine (m^5C) modification, we hypothesized that FTO might participate in the m^6A modification of *Kcnk5*. Additionally, FTO expression was increased in the UIR kidneys *in vivo* and in HK-2 cells treated with TGF-β1 *in vitro* (Figures 7C and 7D). We subsequently confirmed that FTO is restrictively expressed in the proximal tubule and colocalized with TASK-2 by immunofluorescence staining (Figure 7E). It was further proved that FTO was increased in proximal tubules (LTL positive) of patients with renal tubulointerstitial fibrosis (Figure 7F).

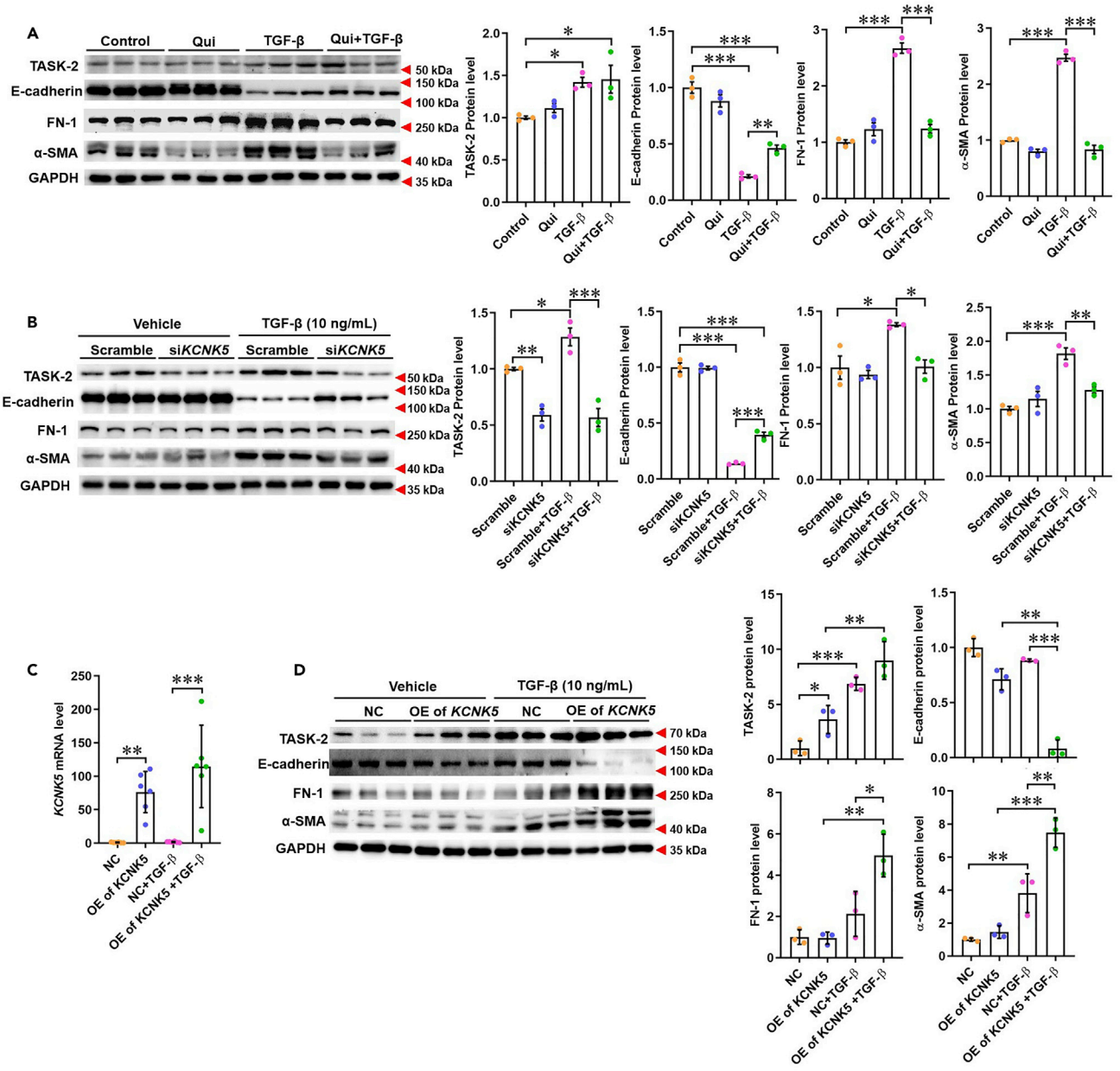

Figure 5. TASK-2 inhibition or *KCNK5* knockdown alleviates fibrogenesis in TGF-β-treated HK-2 cells

(A) Representative western blot analysis of TASK-2, E-cadherin, FN-1, and α-SMA expression in quinidine-treated groups (n = 3).

(B) Representative western blot analysis of TASK-2, E-cadherin, FN-1, and α-SMA expression in si*KCNK5*-treated groups (n = 3).

(C) Real-time qPCR analysis of *KCNK5* mRNA levels in *KCNK5*-overexpression groups (n = 6).

(D) Representative western blot of TASK-2, E-cadherin, FN-1, and α-SMA expression in *KCNK5*-overexpression groups (n = 3).

*p < 0.05, **p < 0.01, ***p < 0.001 by One-way ANOVA, mean ± SD.

To confirm the effect of FTO in the m^{6}A modification of *KCNK5* during renal fibrosis progression, we evaluated this modification by MeRIP-qPCR in MA (an FTO inhibitor)-, TGF-β-, MA + TGF-β-, and vehicle-treated HK-2 cells. We then inhibited FTO by MA treatment at varying concentrations (20, 40, 60, 80, and 100 μM) prior to TGF-β1 treatment (10 ng/mL) for 24 h. The results showed that MA (100 μM) significantly inhibited TGF-β-induced fibrotic changes of HK-2 cells without influencing cell viability (Figures S7A–S7C). Additionally, we found that TGF-β treatment reduced m^{6}A modification of *KCNK5*; however, MA-mediated inhibition of FTO recovered this modification to pretreatment levels (Figures 7G

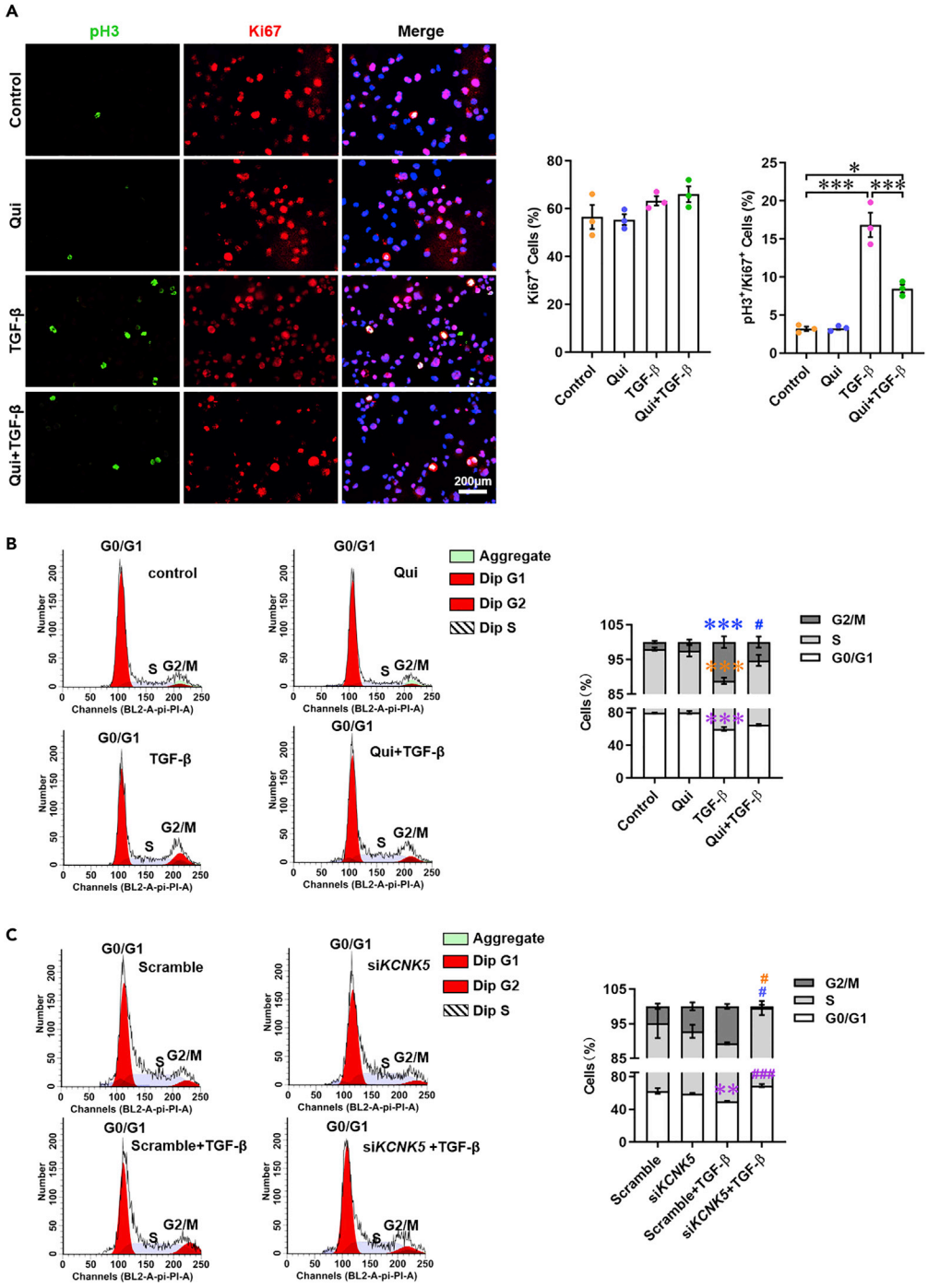

Figure 6. TASK-2 inhibition or *KCNK5* knockdown reduced G2/M cell-cycle arrest in TGF-β-treated HK-2 cells

(A) Representative images of co-immunostaining for pH3 and Ki67 and the percentage of $Ki67^+$ cells and $pH3^+Ki67^+$ cells were counted and calculated in quinidine-treated groups (scale bar 200 μm).

(B and C) Cell cycle analysis was performed by flow cytometry using PI staining in the quinidine-treated (B) and *KNCK5*-knockdown groups (C) prior to statistical analysis of the percentage of cells in the G2/M phase (n = 3). (B and C) $^{**}p < 0.01$, $^{***}p < 0.001$ (vs. the control group), $^{\#}p < 0.05$, $^{\#\#\#}p < 0.001$ (vs. the TGF-β-treated group) by One-way ANOVA, mean ± SD.

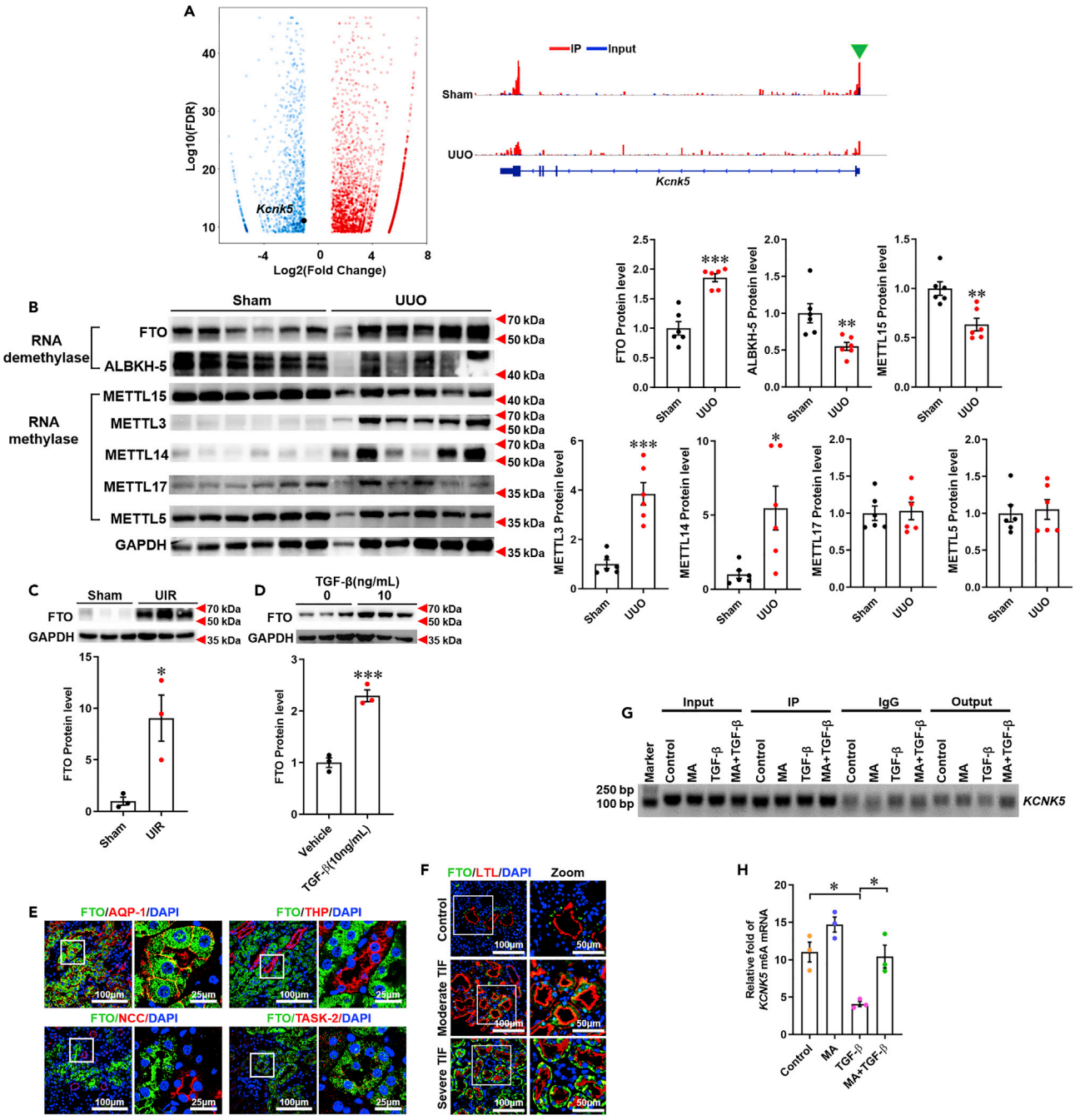

Figure 7. FTO-mediated changes in TASK-2 expression via the m^{6}A modification of *Kcnk5* mRNA and renal fibrosis *in vivo* and *in vitro*

(A) Changes in m^{6}A modifications of *Kcnk5* mRNA in Sham and UUO kidneys according to MeRIP-seq.

(B) Western blot analysis of RNA demethylase and methylase levels in Sham and UUO kidneys (n = 5).

(C) Western blot analysis of FTO in Sham and UIR kidneys (n = 3).

(D) Representative western blot of FTO in vehicle- and TGF-β-treated HK-2 cells (n = 3).

(E) Co-immunostaining for FTO with AQP-1, THP, NCC, and TASK-2 in the kidneys (scale bar 100 μm, zoom 25 μm).

(F) Representative images of FTO co-localization with LTL in human kidneys with tubulointerstitial fibrosis (TIF) (scale bar 100 μm, zoom 50 μm).

(G and H) Level of m^{6}A modification of *KCNK5* evaluated by MeRIP-qPCR in MA-, TGF-β-, MA + TGF-β-, and vehicle-treated HK-2 cells. TGF-β treatment reduced the m^{6}A modification of *KCNK5*; however, inhibiting FTO by MA naturalized this effect. (B–D) *p < 0.05, **p < 0.01, ***p < 0.001 by two-tailed, unpaired *t* test, mean ± SD (H) *p < 0.05 by One-way ANOVA, mean ± SD.

and 7H). These results indicated that the m^{6}A modification of *KCNK5* was altered by elevated FTO during renal fibrosis progression.

Furthermore, we found that mRNA levels of the m^{6}A reader YTH-domain-containing family protein (*YTHDF*)-1 and *YTHDF-2* were increased in the UUO and UIR kidneys and TGF-β-treated HK-2 cells, however, TASK-2 inhibition had no effect on the expression of either *YTHDF*-1 or *YTHDF-2* (Figures S6B–S6D).

Blocking FTO blunted the upregulation of TWIK-related acid-sensitive K$^+$ channel-2, cell-cycle arrest, and renal fibrosis *in vivo* and *in vitro*

To investigate the role of FTO in regulating TASK-2 in renal fibrosis, *Fto* knockdown (*Fto*$^{+/-}$) mice were used since *Fto*-knockout (*Fto*$^{-/-}$) mice are infertile and have a low survival rate. We found that elevated FTO and TASK-2 levels in the UUO- and UIR-kidney were inhibited in *Fto*$^{+/-}$ mice (Figures 8A and 8B). Furthermore, western blot analysis and immunostaining of kidneys from WT and *Fto*$^{+/-}$ mice showed elevations in α-SMA levels were significantly lower in injured kidneys from the *Fto*$^{+/-}$ cohort (Figures 8A–8C). Moreover, the evaluation of fibrotic severity in kidney from WT and *Fto*$^{+/-}$ mice by Masson's trichrome staining at 14 days after UUO and UIR onset revealed attenuated collagen accumulation (blue staining) in kidneys of *Fto*$^{+/-}$ mice (Figure 8D). To clarify the effect of FTO on the cell cycle distribution of proximal tubular epithelial cells *in vivo*, we conducted immunofluorescence staining for Ki67, pH3 and LTL, followed by the calculation of the number of G2/M phase cells (pH3$^+$ and Ki67$^+$) in LTL positive tubules. The accumulation of proliferating renal tubular epithelial cells in the G2/M phase was detected in proximal tubules of UUO-and UIR-kidneys of WT mice, whereas fewer cells in this phase were found in *Fto*$^{+/-}$ mice relative to WT mice (Figure 9).

We then determined the involvement of FTO in regulating TASK-2 activity by treatment with MA and *FTO* siRNA of TGF-β1-stimulated HK-2 cells. The results showed that MA significantly inhibited TGF-β-induced TASK-2 upregulation, fibrotic changes, and intracellular hypokalemia of HK-2 cells (Figures 10A, 10B,and S7A–S7E). To further confirm the effect of FTO, we performed *FTO* silencing and confirmed the subsequent knockdown of FTO levels (Figures S7F and S7G). We observed the same results from FTO inhibition after siRNA-mediated knockdown of FTO levels (Figures 10C, 10D, and S7H). Furthermore, we found that either pharmacological blockage or knockdown of FTO eliminated TGF-β-induced G2/M cell-cycle arrest in HK-2 cells (Figures 11A–11C).

All the results indicated that TASK-2 was upregulated by FTO-mediated *Kcnk5* demethylation and activated by intracellular alkalization, which reduced intracellular K$^+$ concentration, induced G2/M cell-cycle arrest, and aggravated renal fibrosis.

DISCUSSION

Renal fibrosis is the final common manifestation of all forms of progressive renal diseases and results in end-stage renal failure.[29] Chronic fibrotic diseases account for nearly 45% of deaths in developed countries[30]; however, there is no effective therapy for these devastating disorders. To develop effective therapeutic strategies, it is essential to understand the cellular and molecular mechanisms underlying fibrotic development. In this study, we found that TASK-2 level is elevated in renal tubules of mice with UUO- and UIR-induced fibrosis, which was further confirmed in human kidneys with renal tubulointerstitial fibrosis (Figure 1). Conditional knockout of *Kcnk5* in renal epithelium ameliorated kidney fibrosis by reducing G2/M cell-cycle arrest (Figures 2 and 3). Additionally, Kim-1 was elevated in UUO and UIR kidneys, but ablated after *Kcnk5* knockout (Figure 2). Fibrosis often follows the initial injury. Thus, we speculated that *Kcnk5* knockout prevented proximal tubule injury, hence decreased Kim-1, resulting in reduced fibrosis. Proximal tubule cells surviving the injury leads to maladaptive repair with persistent parenchymal inflammation, pericyte/fibroblast proliferation, and excessive deposition of extracellular matrix.[31] In addition, several potassium channels such as KCa3.1 and BK channel were found to participate in kidney fibrosis via influencing TGF-β signaling.[14,32] Therefore TASK-2 maybe also promotes kidney fibrosis via TGF-β signaling, which needs further experiments to verify the speculation. This effect of TASK-2 was subsequently confirmed by TASK-2 inhibition via quinidine or siRNA depletion of *KCNK5* in renal epithelial cells *in vitro* (Figures 4, 5, and 6), and *KCNK5* overexpression resulted in severer fibrotic changes (Figure 5). Notably, TASK-2 expression in the kidney was regulated by RNA demethylase FTO (Figure 7), and either the inhibition or depletion of FTO blunted TASK-2 upregulation and prevented G2/M arrest and fibrotic changes of renal epithelial cells *in vivo* and *in vitro* (Figures 8, 9, 10 and 11). These results indicate that TASK-2 plays a critical

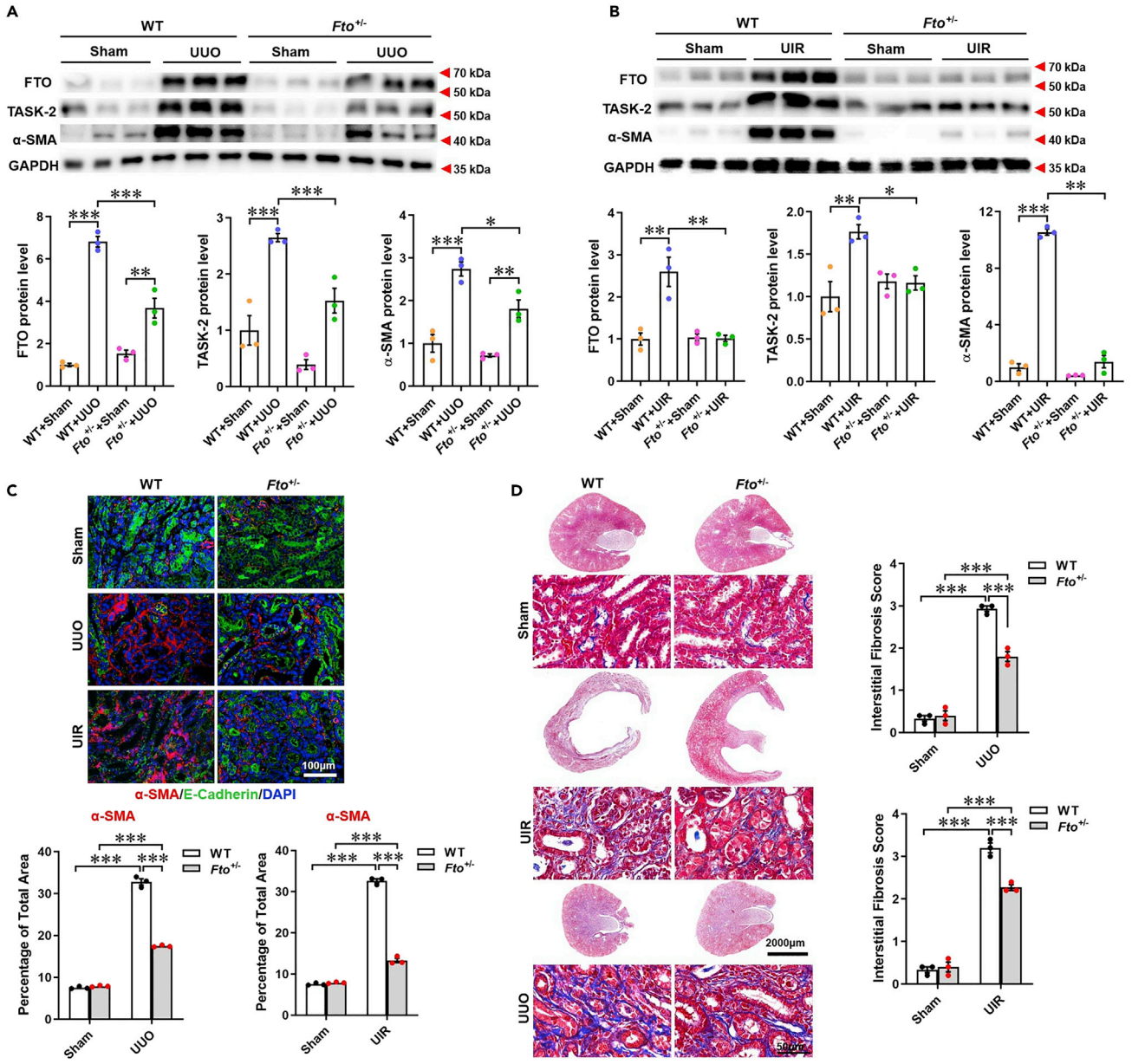

Figure 8. *Fto* knockdown reduces TASK-2 expression and renal fibrosis

Assessment of the degree of tubulointerstitial fibrosis and G2/M cell-cycle arrest in WT and $Fto^{+/-}$ mice 14 days after Sham, UUO, and UIR surgery.

(A) Representative western blot of FTO, TASK-2, and α-SMA expression in UUO mice (n = 3).

(B) Representative western blot of FTO, TASK-2, and α-SMA expression in UIR mice (n = 3).

(C) Immunostaining for α-SMA and E-cadherin (scale bar 100 μm).

(D) Representative images of Masson's trichrome staining (scale bar 2000 μm, zoom 50 μm).

(A and B) *p < 0.05, **p < 0.01, ***p < 0.001 by One-way ANOVA, mean ± SD.

(C and D) ***p < 0.001 by two-way ANOVA, mean ± SD.

role in the progression of tubulointerstitial fibrosis and represents a novel therapeutic target in renal fibrosis.

Potassium is involved in the pathogenic process of renal fibrosis, because chronic potassium depletion induces tubulointerstitial injury.[33] Kidney is the major organ contributing to maintaining K^+ homeostasis. Additionally, K^+ homeostasis is essential to maintaining normal kidney function. Chronic K^+ deficiency

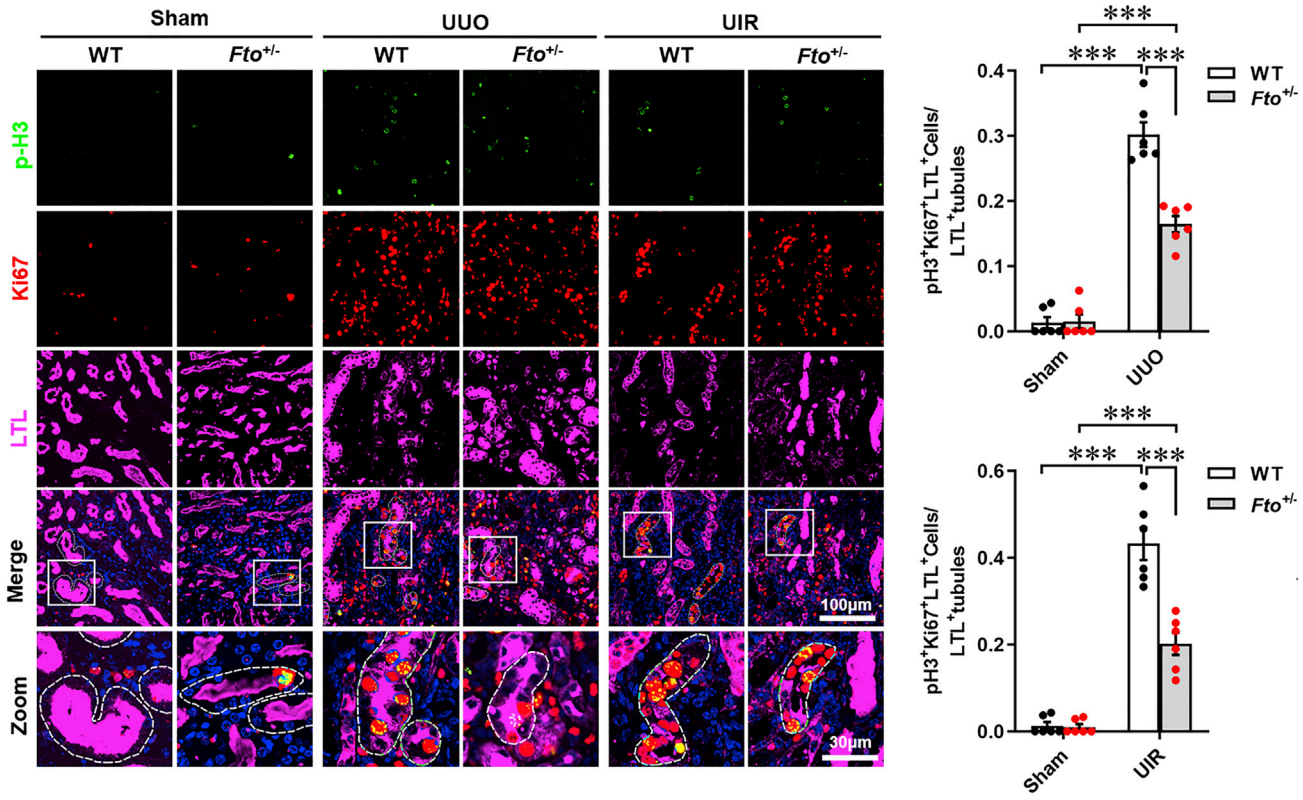

Figure 9. *Fto* knockdown inhibits UUO- and UIR-induced G2/M arrest

Co-immunostaining for pH3 and Ki67 in sham, UUO, and UIR kidneys. (scale bar 100 μm, zoom 30 μm). Counting of $pH3^+Ki67^+LTL^+$ cells in LTL^+ tubules (n = 3 × 2). ***p < 0.001 by two-way ANOVA, mean ± SD.

could cause renal dysfunction and structural changes and facilitate the development of ESRD.[34] The greatest site of injury in hypokalemic nephropathy is the outer medulla, which is characterized by tubular hyperplasia, cell proliferation, and interstitial fibrosis.[35] A previous study reported that targeted disruption of potassium channels, such as the intermediate/small-conductance Ca^{2+}-activated K^+ channel (K(Ca)3.1), attenuated renal fibrosis.[15] TASK-2 widely expressed in renal tubules is a pH-sensitive potassium channel activated by extracellular or intracellular alkaline pH to induce an outward K^+ current, resulting in reduced intracellular K^+ concentration.[36] Besides, TASK-2 was well known for its role in the regulation of immune reaction such as TASK-2 activation promotes effector function in human NK cells and T lymphocytes.[37,38] Since kidney fibrosis was often accompanied by inflammation, TASK-2 may play a role in inflammatory immune responses. However, the role of TASK-2 in the pathogenic progress of renal diseases remains to be elucidated. In the present study, we found identified upregulated TASK-2 expression in renal fibrosis both *in vivo* and *in vitro*. Moreover, we found that TGF-β treatment increased intracellular pH, decreased extracellular pH and intracellular K^+ concentration (Figure 4). This agrees with a previous study reporting that TGF-β treatment elevated intracellular pH, increased net acid extrusion, and epithelial-mesenchymal transition in pancreatic ductal adenocarcinoma cells.[39] These results indicate that TASK-2 activation is characterized by its upregulated expression and function during fibrogenic progression. Furthermore, we found that extracellular alkalosis alone didn't induce fibrotic changes but aggravated TGF-β-induced fibrotic changes of renal epithelial cells, with this process blunted by quinidine-mediated TASK-2 inhibition (Figure 4). These observations suggest that intracellular alkalosis is a potential mechanism responsible for TASK-2 stimulation following TGF-β1 exposure. Although further studies are needed to explore the mechanism of TASK-2 activation, our findings emphasize the role of TASK-2 in renal fibrosis.

A common feature of interstitial fibrosis is epithelial G2/M arrest. Renal insults, such as ischemic, toxicity or obstruction can lead to maladaptive response in tubular epithelial cells. Cells undergoing such a maladaptive response arrest at the G2/M phase as opposed to the G1/0 phase under normal conditions.[40] Cells arresting at the G2/M phase secrete profibrotic factors, such as TGF-β, in a paracrine fashion to act on

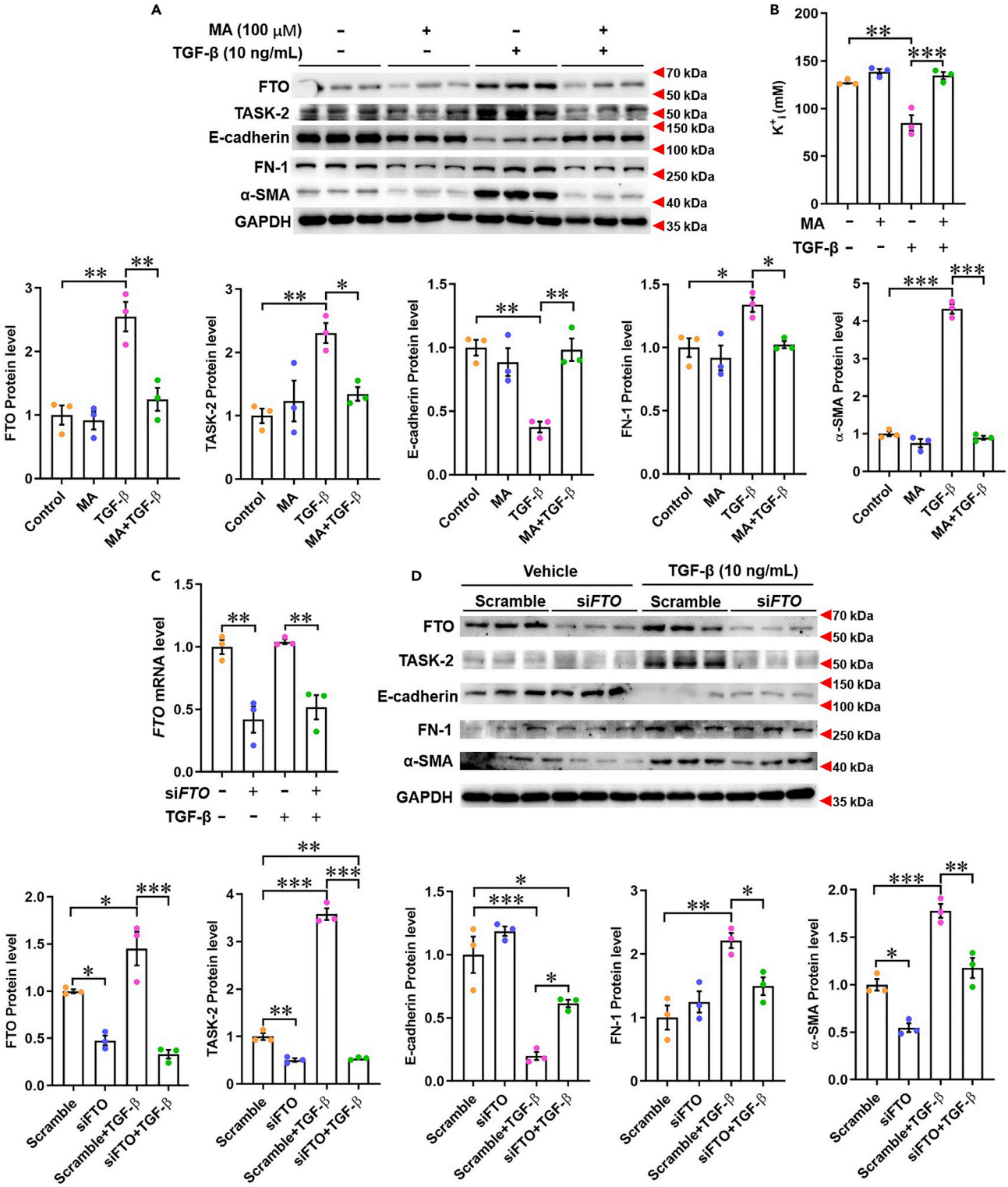

Figure 10. FTO inhibition or *FTO* knockdown reduces TASK-2 expression and fibrogenesis in TGF-β-treated HK-2 cells

HK-2 cells were pretreated with 100 μM MA to pharmacologically inhibit FTO or transfected with *FTO* siRNA prior to exposure to TGF-β (10 ng/mL), and intracellular K^+ concentration, TASK-2 expression, fibrogenesis, and cell cycle progression were measured 24 h after TGF-β treatment.

(A) Representative western blot of FTO, TASK-2, E-cadherin, α-SMA, and FN-1 expression in MA-treated groups (n = 3).

(B) Intracellular K^+ measurements in MA-treated groups (n = 3).

Figure 10. *Continued*

(C) Real-time qPCR analysis of *FTO* mRNA levels in *FTO*-knockdown groups (n = 3).

(D) Representative western blot of FTO, TASK-2, E-cadherin, α-SMA, and FN-1 expression in *FTO*-knockdown groups (n = 3).

*p < 0.05, **p < 0.01, ***p < 0.001 by One-way ANOVA, mean ± SD.

interstitial fibroblasts and accelerate the production of interstitial matrix.[27,41,42] Additionally, a previous study reported that alkalosis (pH7.8) induces G2/M cell-cycle arrest in cortical collecting duct cells *in vitro*.[43] However, whether TASK-2 activation contributes to cell cycle regulation remained unclear. In the present study, we demonstrated that conditional knockout of *KCNK5* in the renal epithelia tubules significantly reduced the UUO- and UIR-induced G2/M cell-cycle arrest and renal fibrosis (Figures 2 and 3). Moreover, *in vitro* epithelial cell culture confirmed that blocking TASK-2 or silencing *KCNK5* reversed TGF-β-induced G2/M arrest of renal epithelial cells (Figure 5). A recent study demonstrated that prolonged K^+ deficiency increased G2/M cell-cycle arrest in renal tubular cells.[44] As the main intracellular ion, K^+ participates in the regulation of cell volume during cell cycle progression.[45] In the present study, the results identified TASK-2 activation and decreases in intracellular K^+ during fibrotic changes of renal tubular epithelial cells, whereas TASK-2 inhibition reversed reduced intracellular K^+ and eliminated G2/M arrest (Figures 4 and 6). These findings indicate that TASK-2 activation leads to reduced intracellular K^+ concentration, which induces G2/M arrest of renal tubular cells and promotes tubulointerstitial fibrosis.

We found inconsistent levels of *Kcnk5* mRNA relative to TASK-2 protein levels in UUO- and UIR-induced renal fibrosis and TGF-β-induced fibrotic changes, indicating the involvement of posttranscriptional regulation (Figures 1 and S3). m6A modifications are the most prevalent posttranscriptional regulation of eukaryotic mRNA.[18] However, it remained unclear whether the modification was present in *Kcnk5*. We recently found that the m6A level was increased in the kidney of UUO model animals (Figure S6). To investigate the role of m6A in renal fibrosis, we employed MeRIP-seq and identified decreased m6A modification of *Kcnk5* was in UUO kidneys and TGF-β-treated HK-2 cells (Figure 7). To clarify the mechanism of the m^6A modification of *Kcnk5*, we detected the expression of demethylases and methyltransferases, finding upregulated levels of the demethylase FTO and the methyltransferases METTL3, METTL14 and decreased levels of the demethylase ALBKH-5 and the methyltransferase METTL15 in the UUO kidneys (Figure 7). This suggested that changes in FTO and METTL15 expression might contribute to the *Kcnk5* demethylation. Because METTL15 mainly functions as an N4-methylcytidine (m^4C) methyltransferase,[46,47] we considered that FTO upregulation might regulate the m^6A modification of *Kcnk5*. Indeed, the data identified FTO and TASK-2 co-localization in renal tubules (Figure 7), and *Fto* knockdown reduced TASK-2 expression, leading to G2/M arrest and renal fibrosis (Figures 8 and 9). FTO inhibition or deficiency prevented the TGF-β-induced TASK-2 upregulation via increased m6A level of *KCNK5* (Figure 7), resulting in intracellular hypokalemia accompanied by the amelioration of G2/M arrest and fibrotic changes of renal epithelial cells (Figures 10 and 11). This agreed with previous studies reporting increased FTO level in UUO kidneys, and that *FTO* silencing attenuated fibrogenic responses.[25,26] Additionally, a population-based case-control study revealed that an FTO polymorphism is associated with CKD.[23]

In the present study, we found that the demethylation of *Kcnk5* mRNA might explain the specific effect of FTO on kidney fibrosis. To investigate how the instability of *Kcnk5* mRNA harboring fewer m6A modifications might result in higher translation efficiency, we analyzed the expression of YTHDF-1 and YTHDF-2, revealing increased levels of both in renal fibrosis (Figure S6). Previous studies reported that the recognition of m6A modifications by YTHDF1 results in enhanced protein synthesis, whereas recognition by YTHDF-2 results in mRNA degradation.[18,48] In this context, we cannot explain how the upregulation of both YTHDF-1 and YTHDF-2 resulted in the observed change in *Kcnk5* stability coupled with translation efficiency in our findings. A previous report indicated that m6A incorporation into mRNA sequences could negatively regulate translation without affecting RNA stability.[49] From this standpoint, demethylation of *Kcnk5* mRNA might promote of its translation to TASK-2; however, further investigations are needed to reveal the precise mechanism.

In conclusion, we demonstrated that TASK-2 induced G2/M cell-cycle arrest and promoted renal fibrosis *in vivo* and *in vitro*, and that TASK-2 blockade by either mRNA silencing or functional inhibition reduced G2/M arrest and renal fibrosis. Furthermore, we identified the upregulation and co-localization of the demethylase FTO and subsequent upregulation of TASK-2 expression, and that *FTO* silencing restored intracellular K^+ concentration, as well as reversed G2/M arrest and fibrotic progression, which was

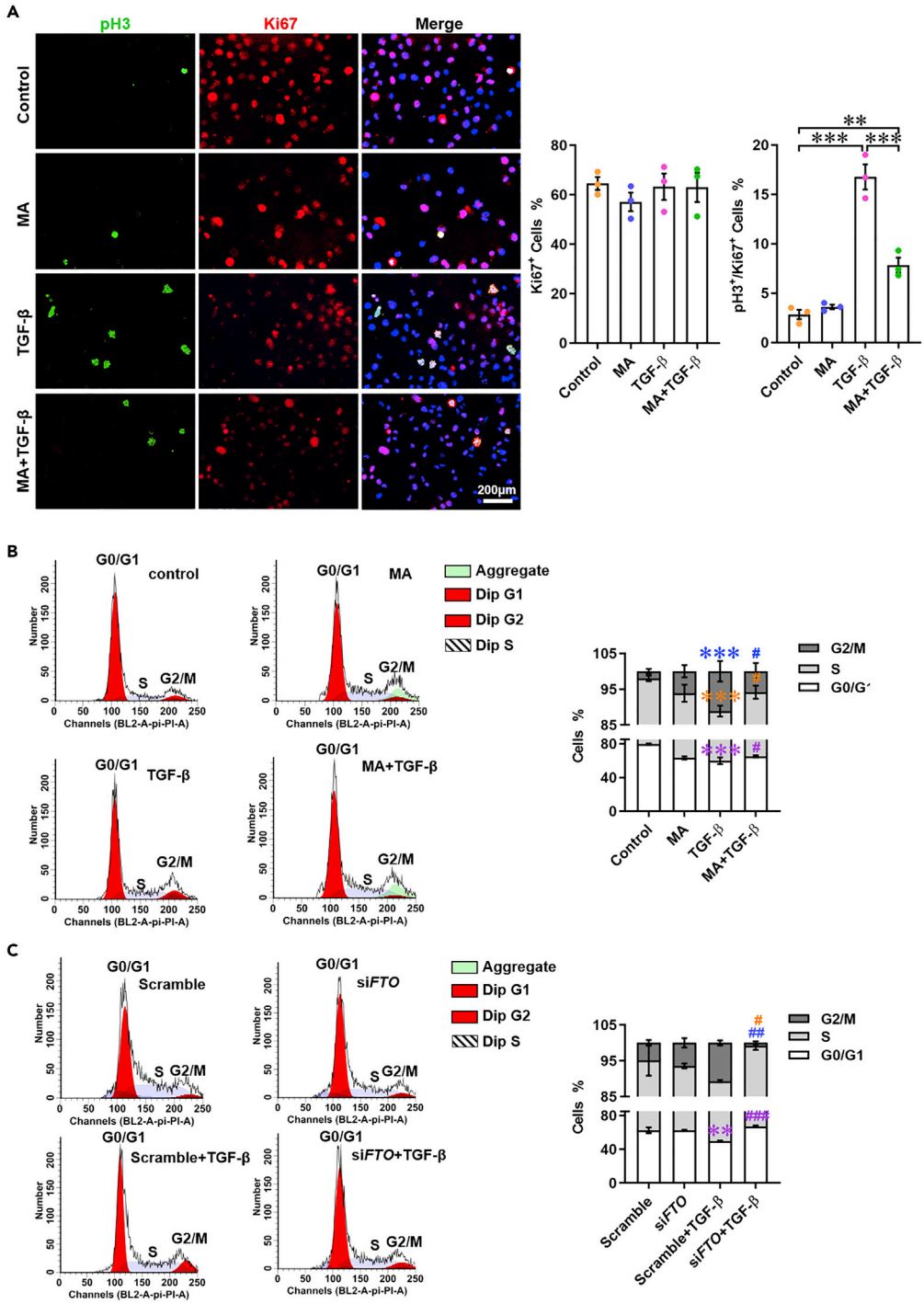

Figure 11. FTO inhibition or *FTO* knockdown suppresses G2/M cell-cycle arrest in TGF-β-treated HK-2 cells

(A) Representative images of co-immunostaining for pH3 and Ki67 and determination of the percentages of $Ki67^+$ and $pH3^+Ki67^+$ cells in MA-treated groups.

(B and C) Cell cycle analysis by flow cytometry using PI staining in MA-treated (B) and *FTO*-knockdown (C) groups.

*p < 0.05, **p < 0.01, ***p < 0.001 vs. the control group; #p < 0.05, ##p < 0.01, ###p < 0.001 vs. the TGF-β group by One-way ANOVA, mean ± SD.

consistent with findings following TASK-2 inhibition. These results strongly support the future investigation of TASK-2 inhibition as a therapeutic strategy to slow CKD progression in patients.

Limitations of the study

Our study demonstrated that the upregulation of TASK-2 via FTO-mediated m6A modification on *Kcnk5* mRNA promotes renal fibrosis by inducing G2/M cell-cycle arrest in proximal tubular cells, making TASK-2 a promising target for diagnosis and treatment for renal fibrosis in patients with CKD. However, the mechanism of how TASK-2 induces G2/M cell-cycle arrest in proximal tubular cells needs further investigation. In addition, although we used $Kcnk5^{fl/fl}/Cdh16^{cre}$ mice to prove that knockout of TASK-2 in proximal tubules alleviated G2/M cell-cycle arrest and renal fibrosis, it is better to be evaluated in $Kcnk5^{fl/fl}/Kap^{cre}$ mice which are currently unavailable.

DATA SHARING STATEMENT

All data will be made available by the corresponding author upon reasonable request.

STAR★METHODS

Detailed methods are provided in the online version of this paper and include the following:

- KEY RESOURCES TABLE
- RESOURCE AVAILABILITY
  - Lead contact
  - Materials availability
  - Data and code availability
- EXPERIMENTAL MODELS AND SUBJECT DETAILS
  - Animals
  - Animal models
  - Human kidney samples
  - Cell lines
  - Study approval
- METHOD DETAILS
  - Methylated RNA immunoprecipitation sequencing (MeRIP-seq) and data analysis
  - MeRIP-quantitative (q)PCR
  - Histopathological examinations and immunofluorescence staining
  - Cell treatments
  - Western blotting
  - Real-time quantitative PCR
  - Wound healing
  - CCK-8 assay
  - Intracellular pH and potassium measurement
  - Propidium iodide (PI) staining
- QUANTIFICATION AND STATISTICAL ANALYSIS

SUPPLEMENTAL INFORMATION

Supplemental information can be found online at https://doi.org/10.1016/j.isci.2022.105620.

ACKNOWLEDGMENTS

We thank professor Jing Huang (State Key Laboratory of Chemo/Biosensing and Chemometrics, College of Chemistry and Chemical Engineering, Key Laboratory for Bio-Nanotechnology and Molecular Engineering of Hunan Province, Hunan University) and professor Yanjing Yang (College of Chemistry and Chemical Engineering, Central South University) for providing aptamer-based FRET nanoflares K^+ probe (AuNPs@aptamer). This work was supported by grants from the National Natural Science Foundation of China (82070710, 81670614, 81800592, and 81803880), Shanghai Science and Technology Innovation Action Plan (21S21902900, 19DZ2205600 and 21002411500), Shanghai Key Laboratory of Kidney and Blood Purification, Shanghai Science and Technology Commission (20DZ2271600), Shanghai Sailing Program (18YF1419800) and Shanghai Municipal Hospital Frontier Technology Project supported by Shanghai Shen Kang Hospital Development Center (SHDC12018127, SHDC2202230).

AUTHOR CONTRIBUTIONS

NNS and XQD conceived and designed the project. JZ, JC, YFL, YY, WZC, BS, JCH, PJ, YF, SZ, YD, XYZ, MX, and YT contributed to the experimental design. JZ, JC, YFL, YY, WZC, SJX, YQS, YCN, and JLW performed experiments. NNS, JZ, JC, YFL, and YY performed *in vivo* experiments. YQS, YCN, and JLW performed pathologic analysis of blinded kidney samples. WZC, BS, JCH, SJX, and SZ performed *in vitro* experiments. ZCL performed synthesis of pH-sensitive probe. YY and YFL provided materials. NNS and YL performed data analysis. JC is designated the first co-author, as she performed MeRIP-seq and data analysis; YFL is designated the second co-author, as she began the project and perform all long-term *in vivo* experiments. All authors participated in the preparation of the article. All authors read the article, provided feedback and approved the final article.

DECLARATION OF INTERESTS

The authors declare no competing interests.

Received: May 5, 2022
Revised: October 24, 2022
Accepted: November 15, 2022
Published: December 22, 2022

REFERENCES

1. Nastase, M.V., Zeng-Brouwers, J., Wygrecka, M., and Schaefer, L. (2018). Targeting renal fibrosis: mechanisms and drug delivery systems. Adv. Drug Deliv. Rev. *129*, 295–307. https://doi.org/10.1016/j.addr.2017.12.019.

2. Abraham, D.M., Lee, T.E., Watson, L.J., Mao, L., Chandok, G., Wang, H.G., Frangakis, S., Pitt, G.S., Shah, S.H., Wolf, M.J., and Rockman, H.A. (2018). The two-pore domain potassium channel TREK-1 mediates cardiac fibrosis and diastolic dysfunction. J. Clin. Invest. *128*, 4843–4855. https://doi.org/10.1172/jci95945.

3. Lovisa, S., LeBleu, V.S., Tampe, B., Sugimoto, H., Vadnagara, K., Carstens, J.L., Wu, C.C., Hagos, Y., Burckhardt, B.C., Pentcheva-Hoang, T., et al. (2015). Epithelial-to-mesenchymal transition induces cell cycle arrest and parenchymal damage in renal fibrosis. Nat. Med. *21*, 998–1009. https://doi.org/10.1038/nm.3902.

4. Kieneker, L.M., Bakker, S.J.L., de Boer, R.A., Navis, G.J., Gansevoort, R.T., and Joosten, M.M. (2016). Low potassium excretion but not high sodium excretion is associated with increased risk of developing chronic kidney disease. Kidney Int. *90*, 888–896. https://doi.org/10.1016/j.kint.2016.07.012.

5. Picard, K., Barreto Silva, M.I., Mager, D., and Richard, C. (2020). Dietary potassium intake and risk of chronic kidney disease progression in predialysis patients with chronic kidney disease: a systematic review. Adv. Nutr. *11*, 1002–1015. https://doi.org/10.1093/advances/nmaa027.

6. Burnier, M. (2020). Increasing potassium intake to prevent kidney damage: a new population strategy? Kidney Int. *98*, 59–61. https://doi.org/10.1016/j.kint.2020.04.014.

7. Pere, A.K., Lindgren, L., Tuomainen, P., Krogerus, L., Rauhala, P., Laakso, J., Karppanen, H., Vapaatalo, H., Ahonen, J., and Mervaala, E.M. (2000). Dietary potassium and magnesium supplementation in cyclosporine-induced hypertension and nephrotoxicity. Kidney Int. *58*, 2462–2472. https://doi.org/10.1046/j.1523-1755.2000.00429.x.

8. Wang, W., Soltero, L., Zhang, P., Huang, X.R., Lan, H.Y., and Adrogue, H.J. (2007). Renal inflammation is modulated by potassium in chronic kidney disease: possible role of Smad7. Am. J. Physiol. Renal Physiol. *293*, F1123–F1130. https://doi.org/10.1152/ajprenal.00104.2007.

9. Urrego, D., Tomczak, A.P., Zahed, F., Stühmer, W., and Pardo, L.A. (2014). Potassium channels in cell cycle and cell proliferation. Philos. Trans. R. Soc. Lond. B Biol. Sci. *369*, 20130094. https://doi.org/10.1098/rstb.2013.0094.

10. Song, N., Lu, Z., Zhang, J., Shi, Y., Ning, Y., Chen, J., Jin, S., Shen, B., Fang, Y., Zou, J., et al. (2019). Acid-sensing ion channel 1a is involved in ischaemia/reperfusion induced kidney injury by increasing renal epithelia cell apoptosis. J. Cell Mol. Med. *23*, 3429–3440. https://doi.org/10.1111/jcmm.14238.

11. Tao, R., Lau, C.P., Tse, H.F., and Li, G.R. (2008). Regulation of cell proliferation by intermediate-conductance Ca2+-activated potassium and volume-sensitive chloride channels in mouse mesenchymal stem cells. Am. J. Physiol. Cell Physiol. *295*, C1409–C1416. https://doi.org/10.1152/ajpcell.00268.2008.

12. Wonderlin, W.F., and Strobl, J.S. (1996). Potassium channels, proliferation and G1 progression. J. Membr. Biol. *154*, 91–107. https://doi.org/10.1007/s002329900135.

13. Menè, P., and Pirozzi, N. (2013). Potassium channels, renal fibrosis, and diabetes. Diabetes *62*, 2648–2650. https://doi.org/10.2337/db13-0603.

14. Huang, C., Shen, S., Ma, Q., Chen, J., Gill, A., Pollock, C.A., and Chen, X.M. (2013). Blockade of KCa3.1 ameliorates renal fibrosis through the TGF-β1/Smad pathway in diabetic mice. Diabetes *62*, 2923–2934. https://doi.org/10.2337/db13-0135.

15. Grgic, I., Kiss, E., Kaistha, B.P., Busch, C., Kloss, M., Sautter, J., Müller, A., Kaistha, A., Schmidt, C., Raman, G., et al. (2009). Renal fibrosis is attenuated by targeted disruption of KCa3.1 potassium channels. Proc. Natl. Acad. Sci. USA *106*, 14518–14523. https://doi.org/10.1073/pnas.0903458106.

16. Warth, R., Barrière, H., Meneton, P., Bloch, M., Thomas, J., Tauc, M., Heitzmann, D., Romeo, E., Verrey, F., Mengual, R., et al. (2004). Proximal renal tubular acidosis in TASK2 K+ channel-deficient mice reveals a mechanism for stabilizing bicarbonate transport. Proc. Natl. Acad. Sci. USA *101*, 8215–8220. https://doi.org/10.1073/pnas.0400081101.

17. Barriere, H., Belfodil, R., Rubera, I., Tauc, M., Lesage, F., Poujeol, C., Guy, N., Barhanin, J., and Poujeol, P. (2003). Role of TASK2 potassium channels regarding volume regulation in primary cultures of mouse proximal tubules. J. Gen. Physiol. *122*, 177–190. https://doi.org/10.1085/jgp.200308820.

18. Wang, X., Zhao, B.S., Roundtree, I.A., Lu, Z., Han, D., Ma, H., Weng, X., Chen, K., Shi, H., and He, C. (2015). N(6)-methyladenosine modulates messenger RNA translation efficiency. Cell *161*, 1388–1399. https://doi.org/10.1016/j.cell.2015.05.014.

19. Shi, H., Wei, J., and He, C. (2019). Where, when, and how: context-dependent functions of RNA methylation writers, readers, and erasers. Mol. Cell *74*, 640–650. https://doi.org/10.1016/j.molcel.2019.04.025.

20. Zhou, P., Wu, M., Ye, C., Xu, Q., and Wang, L. (2019). Meclofenamic acid promotes cisplatin-induced acute kidney injury by inhibiting fat mass and obesity-associated protein-mediated m(6)A abrogation in RNA. J. Biol. Chem. *294*, 16908–16917. https://doi.org/10.1074/jbc.RA119.011009.

21. Wang, J., Ishfaq, M., Xu, L., Xia, C., Chen, C., and Li, J. (2019). METTL3/m(6)A/miRNA-873-5p attenuated oxidative stress and apoptosis in colistin-induced kidney injury by modulating keap1/Nrf2 pathway. Front. Pharmacol. *10*, 517. https://doi.org/10.3389/fphar.2019.00517.

22. Xu, Y., Yuan, X.D., Wu, J.J., Chen, R.Y., Xia, L., Zhang, M., Han, C.H., and Mou, S. (2020). The N6-methyladenosine mRNA methylase METTL14 promotes renal ischemic reperfusion injury via suppressing YAP1. J. Cell. Biochem. *121*, 524–533. https://doi.org/10.1002/jcb.29258.

23. Hubacek, J.A., Viklicky, O., Dlouha, D., Bloudickova, S., Kubinova, R., Peasey, A., Pikhart, H., Adamkova, V., Brabcova, I., Pokorna, E., and Bobak, M. (2012). The FTO gene polymorphism is associated with end-stage renal disease: two large independent case-control studies in a general population. Nephrol. Dial. Transplant. *27*, 1030–1035. https://doi.org/10.1093/ndt/gfr418.

24. Liu, P., Zhang, B., Chen, Z., He, Y., Du, Y., Liu, Y., and Chen, X. (2020). m(6)A-induced lncRNA MALAT1 aggravates renal fibrogenesis in obstructive nephropathy through the miR-145/FAK pathway. Aging *12*, 5280–5299. https://doi.org/10.18632/aging.102950.

25. Wang, C.Y., Shie, S.S., Tsai, M.L., Yang, C.H., Hung, K.C., Wang, C.C., Hsieh, I.C., and Wen, M.S. (2016). FTO modulates fibrogenic responses in obstructive nephropathy. Sci. Rep. *6*, 18874. https://doi.org/10.1038/srep18874.

26. Li, X., Fan, X., Yin, X., Liu, H., and Yang, Y. (2020). Alteration of N(6)-methyladenosine epitranscriptome profile in unilateral ureteral obstructive nephropathy. Epigenomics *12*, 1157–1173. https://doi.org/10.2217/epi-2020-0126.

27. Yang, L., Besschetnova, T.Y., Brooks, C.R., Shah, J.V., and Bonventre, J.V. (2010). Epithelial cell cycle arrest in G2/M mediates kidney fibrosis after injury. Nat. Med. *16*, 535–543. https://doi.org/10.1038/nm.2144.

28. Courtney, D.G. (2021). Post-transcriptional regulation of viral RNA through epitranscriptional modification. Cells *10*, 1129. https://doi.org/10.3390/cells10051129.

29. Shen, Y., Miao, N., Wang, B., Xu, J., Gan, X., Xu, D., Zhou, L., Xue, H., Zhang, W., Yang, L., and Lu, L. (2017). c-Myc promotes renal fibrosis by inducing integrin αv-mediated transforming growth factor-β signaling. Kidney Int. *92*, 888–899. https://doi.org/10.1016/j.kint.2017.03.006.

30. Friedman, S.L., Sheppard, D., Duffield, J.S., and Violette, S. (2013). Therapy for fibrotic diseases: nearing the starting line. Sci. Transl. Med. *5*, 167sr1. https://doi.org/10.1126/scitranslmed.3004700.

31. Canaud, G., Brooks, C.R., Kishi, S., Taguchi, K., Nishimura, K., Magassa, S., Scott, A., Hsiao, L.L., Ichimura, T., Terzi, F., et al. (2019). Cyclin G1 and TASCC regulate kidney epithelial cell G(2)-M arrest and fibrotic maladaptive repair. Sci. Transl. Med. *11*, eaav4754. https://doi.org/10.1126/scitranslmed.aav4754.

32. Wang, Y., Wang, M., Ning, F., Ren, D., Tao, J., Xie, W., Eaton, D.C., Jiang, G., Farris, A.B., Xin, H., et al. (2022). A novel role of BK potassium channel activity in preventing the development of kidney fibrosis. Kidney Int. *101*, 945–962. https://doi.org/10.1016/j.kint.2021.11.033.

33. Ray, P.E., Suga, S., Liu, X.H., Huang, X., and Johnson, R.J. (2001). Chronic potassium depletion induces renal injury, salt sensitivity, and hypertension in young rats. Kidney Int. *59*, 1850–1858. https://doi.org/10.1046/j.1523-1755.2001.0590051850.x.

34. Menahem, S.A., Perry, G.J., Dowling, J., and Thomson, N.M. (1999). Hypokalaemia-induced acute renal failure. Nephrol. Dial. Transplant. *14*, 2216–2218. https://doi.org/10.1093/ndt/14.9.2216.

35. Reungjui, S., Roncal, C.A., Sato, W., Glushakova, O.Y., Croker, B.P., Suga, S.I., Ouyang, X., Tungsanga, K., Nakagawa, T., Johnson, R.J., and Mu, W. (2008). Hypokalemic nephropathy is associated with impaired angiogenesis. J. Am. Soc. Nephrol. *19*, 125–134. https://doi.org/10.1681/asn.2007030261.

36. Niemeyer, M.I., Cid, L.P., Peña-Münzenmayer, G., and Sepúlveda, F.V. (2010). Separate gating mechanisms mediate the regulation of K2P potassium channel TASK-2 by intra- and extracellular pH. J. Biol. Chem. *285*, 16467–16475. https://doi.org/10.1074/jbc.M110.107060.

37. Schulte-Mecklenbeck, A., Bittner, S., Ehling, P., Döring, F., Wischmeyer, E., Breuer, J., Herrmann, A.M., Wiendl, H., Meuth, S.G., and Gross, C.C. (2015). The two-pore domain K2 P channel TASK2 drives human NK-cell proliferation and cytolytic function. Eur. J. Immunol. *45*, 2602–2614. https://doi.org/10.1002/eji.201445208.

38. Fernández-Orth, J., Ehling, P., Ruck, T., Pankratz, S., Hofmann, M.S., Landgraf, P., Dieterich, D.C., Smalla, K.H., Kähne, T., Seebohm, G., et al. (2017). 14-3-3 Proteins regulate K2P 5.1 surface expression on T lymphocytes. Traffic *18*, 29–43. https://doi.org/10.1111/tra.12455.

39. Malinda, R.R., Zeeberg, K., Sharku, P.C., Ludwig, M.Q., Pedersen, L.B., Christensen, S.T., and Pedersen, S.F. (2020). TGFβ signaling increases net acid extrusion, proliferation and invasion in panc-1 pancreatic cancer cells: SMAD4 dependence and link to merlin/NF2 signaling. Front. Oncol. *10*, 687. https://doi.org/10.3389/fonc.2020.00687.

40. Tan, H.L., Yap, J.Q., and Qian, Q. (2016). Acute kidney injury: tubular markers and risk for chronic kidney disease and end-stage kidney failure. Blood Purif. *41*, 144–150. https://doi.org/10.1159/000441269.

41. Canaud, G., and Bonventre, J.V. (2015). Cell cycle arrest and the evolution of chronic kidney disease from acute kidney injury. Nephrol. Dial. Transplant. *30*, 575–583. https://doi.org/10.1093/ndt/gfu230.

42. Wu, C.F., Chiang, W.C., Lai, C.F., Chang, F.C., Chen, Y.T., Chou, Y.H., Wu, T.H., Linn, G.R., Ling, H., Wu, K.D., et al. (2013). Transforming growth factor β-1 stimulates profibrotic epithelial signaling to activate pericyte-myofibroblast transition in obstructive kidney fibrosis. Am. J. Pathol. *182*, 118–131. https://doi.org/10.1016/j.ajpath.2012.09.009.

43. Rivarola, V., Flamenco, P., Melamud, L., Galizia, L., Ford, P., and Capurro, C. (2010). Adaptation to alkalosis induces cell cycle delay and apoptosis in cortical collecting duct cells: role of Aquaporin-2. J. Cell. Physiol. *224*, 405–413. https://doi.org/10.1002/jcp.22136.

44. Fong-Ngern, K., Ausakunpipat, N., Singhto, N., Sueksakit, K., and Thongboonkerd, V. (2017). Prolonged K(+) deficiency increases intracellular ATP, cell cycle arrest and cell death in renal tubular cells. Metabolism *74*, 47–61. https://doi.org/10.1016/j.metabol.2016.12.014.

45. Marakhova, I., Domnina, A., Shatrova, A., Borodkina, A., Burova, E., Pugovkina, N., Zemelko, V., and Nikolsky, N. (2019). Proliferation-related changes in K(+) content in human mesenchymal stem cells. Sci. Rep. *9*, 346. https://doi.org/10.1038/s41598-018-36922-y.

46. Van Haute, L., Hendrick, A.G., D'Souza, A.R., Powell, C.A., Rebelo-Guiomar, P., Harbour, M.E., Ding, S., Fearnley, I.M., Andrews, B., and Minczuk, M. (2019). METTL15 introduces N4-methylcytidine into human mitochondrial 12S rRNA and is required for mitoribosome biogenesis. Nucleic Acids Res. *47*, 10267–10281. https://doi.org/10.1093/nar/gkz735.

47. Laptev, I., Shvetsova, E., Levitskii, S., Serebryakova, M., Rubtsova, M., Zgoda, V., Bogdanov, A., Kamenski, P., Sergiev, P., and Dontsova, O. (2020). METTL15 interacts with the assembly intermediate of murine mitochondrial small ribosomal subunit to form m4C840 12S rRNA residue. Nucleic Acids Res. *48*, 8022–8034. https://doi.org/10.1093/nar/gkaa522.

48. Wang, X., Lu, Z., Gomez, A., Hon, G.C., Yue, Y., Han, D., Fu, Y., Parisien, M., Dai, Q., Jia, G., et al. (2014). N6-methyladenosine-dependent regulation of messenger RNA stability. Nature *505*, 117–120. https://doi.org/10.1038/nature12730.

49. Zhou, J., Wan, J., Shu, X.E., Mao, Y., Liu, X.M., Yuan, X., Zhang, X., Hess, M.E., Brüning, J.C., and Qian, S.B. (2018). N(6)-Methyladenosine guides mRNA alternative translation during integrated stress

response. Mol. Cell *69*, 636–647.e7. https://doi.org/10.1016/j.molcel.2018.01.019.

50. Bolger, A.M., Lohse, M., and Usadel, B. (2014). Trimmomatic: a flexible trimmer for Illumina sequence data. Bioinformatics *30*, 2114–2120. https://doi.org/10.1093/bioinformatics/btu170.

51. Kim, D., Paggi, J.M., Park, C., Bennett, C., and Salzberg, S.L. (2019). Graph-based genome alignment and genotyping with HISAT2 and HISAT-genotype. Nat. Biotechnol. *37*, 907–915. https://doi.org/10.1038/s41587-019-0201-4.

52. Feng, J., Liu, T., Qin, B., Zhang, Y., and Liu, X.S. (2012). Identifying ChIP-seq enrichment using MACS. Nat. Protoc. *7*, 1728–1740. https://doi.org/10.1038/nprot.2012.101.

53. Machanick, P., and Bailey, T.L. (2011). MEME-ChIP: motif analysis of large DNA datasets. Bioinformatics *27*, 1696–1697. https://doi.org/10.1093/bioinformatics/btr189.

54. Kong, B., Zhu, A., Ding, C., Zhao, X., Li, B., and Tian, Y. (2012). Carbon dot-based inorganic-organic nanosystem for two-photon imaging and biosensing of pH variation in living cells and tissues. Adv. Mater. *24*, 5844–5848. https://doi.org/10.1002/adma.201202599.

55. Yang, Y., Huang, J., Yang, X., Quan, K., Xie, N., Ou, M., Tang, J., and Wang, K. (2016). Aptamer-based FRET nanoflares for imaging potassium ions in living cells. Chem. Commun. *52*, 11386–11389. https://doi.org/10.1039/c6cc05379c.

STAR★METHODS

KEY RESOURCES TABLE

REAGENT or RESOURCE	SOURCE	IDENTIFIER
Antibodies		
Anti-KCNK5(TASK-2) antibody	alomone lab	Cat#: APC-037; RRID: AB_2040134
TASK-2(G-14)	Santa Cruz	Cat#: sc-11314; RRID: AB_2265298
Anti-KCNK5 antibody	Merck	Cat#: HPA059148; RRID:AB_2683929
Anti-N6-methyladenosine (m6A) antibody [17-3-4-1]	Abcam	Cat#: ab208577; RRID:AB_2916290
Anti-Aquaporin 1 (AQP1) antibody [EPR11588(B)]	Abcam	Cat#: ab168387; RRID: AB_2810992
Anti-Thiazide-Sensitive NaCl Cotransporter (NCC) Antibody	EMD Millipore	Cat#: AB3553; RRID: AB_571116
Anti-Uromucoid (THP) antibody [EPR20071]	Abcam	Cat#: ab207170; RRID: AB_2889163
Anti-Aquaporin 2 (AQP2) antibody [EPR21080]	Merck	Cat#: AB3274; RRID: AB_2889163
Anti-Histone H3 (phospho S10)	Abcam	Cat#: ab14955; RRID: AB_443110
Ki-67 (D3B5) Rabbit mAb	Cell Signaling Technology	Cat#: 9129; RRID: AB_2687446
Anti-LTL antibody	Vector	Cat#: B-1325; RRID: AB_2336558
Anti-ailpha smooth muscle Actin (α-SMA) antibody[E184]	Abcam	Cat#: ab32575; RRID: AB_722538
Purified Mouse Anti-E-Cadherin	BD Bioscience	Cat#: 610181; RRID: AB_397580
Anti-FTO antibody [5-2H10]	Abcam	Cat#: ab92821; RRID: AB_10565042
Anti-ALKBH5 antibody [EPR18958]	Abcam	Cat#: ab234528; RRID: AB_2924923
Anti-METTL3 antibody [EPR18810]	Abcam	Cat#: ab195352; RRID: AB_2721254
METTL5 Polyclonal antibody	Proteintech	Cat#: 16791-1-AP; RRID: AB_2142051
Anti-METTL14 antibody	Abcam	Cat#: ab252562; RRID: AB_2924924
Anti-METT5D1 (METTL15) antibody	Abcam	Cat#: ab220228; RRID: AB_2924925
METTL7B Antibody	Proteintech	Cat#: 17001-1-AP; RRID: AB_2142199
FN1 Polyclonal Antibody	IMMUNOWAY	Cat#: YT1733; RRID: AB_2924926
Anti-GAPDH antibody [6C5]	Abcam	Cat#: ab8245; RRID: AB_2107448
Biological samples		
Human kidney samples	Zhongshan Hospital, Fudan University	N/A
Chemicals, peptides, and recombinant proteins		
meclofenamic acid	CSNpharm	Cat#: CSN24828
quinidine	CSNpharm	Cat#: CSN11818
clofilium	CSNpharm	Cat#: C335117
Trizol reagent	Invitrogen	Cat#: 15596018
Dynabeads Protein A	Invitrogen	Cat#: 10001D
valinomycin	Aladdin Bio-Chem Technology Co.	Cat#: V100895
nigericin	Aladdin Bio-Chem Technology Co.	Cat#: N102401
carbon dot-based inorganic–organic pH-sensitive probe (CDs@FITC)	Dr. Tian, Yang	N/A
aptamer-based FRET nanoflare K+ probe (AuNPs@aptamer)	Dr. Huang, Jing	N/A
KCNK5 siRNA	Genepharma	This Paper Table S1

(*Continued on next page*)

Continued

REAGENT or RESOURCE	SOURCE	IDENTIFIER
FTO siRNA	Genepharma	This Paper Table S1
Scramble siRNA	Genepharma	This Paper Table S1
Critical commercial assays		
KAPA stranded mRNA-seq kit	Illumina	Cat#: KK8421
NovaSeq 6000 S4 reagent kit	Illumina	Cat#: 20028312
Masson's trichrome stain kit	Solarbio@LIFE SCIENCE	Cat#: G1340
PrimeScript™ RT Master Mix	Takara	Cat#: RR036A
TB Green™ Premix Ex Taq™ II (Tli RNaseH Plus)	Takara	Cat#: RR820A
Lipofectamine 3000 Transfection Reagent	Invitrogen	Cat#: L3000001
CCK-8 assay	Dojindo	Cat#: CK04
cell cycle detection kit	Keygen	Cat#: KGA511
Deposited data		
MeRIP-seq	DRYAD	Mendeley Data: https://doi.org/10.5061/dryad.r2280gbbz
Experimental models: Cell lines		
HK-2 cells	ATCC	Cat# CRL-2190, RRID: CVCL_0302
Experimental models: Organisms/strains		
$Kcnk5^{flox/flox}$	This study	N/A
$Cdh16^{cre}$	Cyagen	Name: C57BL/6J-Cdh16em1cyagen, Serial Number: KOCMP-12556-Cdh16-B6J-VA
$FTO^{-/-}$	Cyagen	Name: C57BL/6J-$Fto^{em1cyagen}$, Serial Number: KOCMP-26383-Fto-B6J-VA
Oligonucleotides		
Primers	This Paper	This Paper Table S2
Software and algorithms		
Flowjo	Flowjo software	Version 10
ImageJ	ImageJ software	Version 1.52
Graphpad Prism	Graphpad software	Version 8.2.0
Photoshop CS6 Extended	Adobe	N/A
Trimmomatic software	Reference Bolger et al.[50]	http://www.usadellab.org/cms/?page=trimmomatic
HISAT2 software	Reference Kim et al.[51]	https://daehwankimlab.github.io/hisat2/
Model-based analysis of ChIP-seq (MACS)	Reference Feng et al.[52]	http://liulab.dfci.harvard.edu/MACS/
MEME-ChIP	Reference Machanick and Bailey,[53]	http://meme.nbcr.net/

RESOURCE AVAILABILITY

Lead contact

Further information and requests for resources and reagents should be directed to and will be fulfilled by the lead contact, Xiaoqiang Ding (ding.xiaoqiang@zs-hospital.sh.cn).

Materials availability

This study did not generate new unique materials.

Data and code availability

- MeRIP-seq data has been uploaded to DRYAD and are publicly available (Mendeley Data: https://doi.org/10.5061/dryad.r2280gbbz).

- This paper does not report original code.
- Any additional information required to reanalyze the data reported in this paper is available from the lead contact upon request.

EXPERIMENTAL MODELS AND SUBJECT DETAILS

Animals

Generation of renal tubular-specific Kcnk5 knockout mice

We used the Cre/loxP recombination system to generate tubule-specific *Kcnk5*-deletion (*Kcnk5*$^{flox/flox}$/*Cdh16*^{cre}) mice (Cyagen, Santa Clara, CA, USA). Mice maintained on the C57BL/6 background with the *Kcnk5*-floxed allele were crossed with mice expressing Cre recombinase under the cadherin 16 promoter (*Cdh16*^{Cre}). PCR, immunofluorescence staining, and western blot were performed to clarify the genotype. The *Kcnk5*$^{flox/flox}$ and wild-type (WT) alleles were detected using the following primers: 5′-ACTTCTTGG AAACCACATGGAAAC-3′ and 5′-AATGATCTACTCAGGTCCACACAG-3′, which generated a 212-bp product in the floxed allele and a 167-bp product in the WT allele. The *Cdh16*-Cre transgene was detected using the primers 5′- GCAGATCTGGCTCTCCAAAG-3′ and 5′- AGGCAAATTTTGGTGTACGG-3′, which amplified a 420-bp fragment. C57BL/6 wide-type (WT) mice, floxed without *Cdh16*-Cre (*Kcnk5*$^{flox/flox}$) mice, served as the control group.

Fto knockdown mice

Fto-heterozygous (*Fto*$^{+/-}$) mice bred on a pure C57BL/6J background were used since *Fto*-knockout (*Fto*$^{-/-}$) mice are infertile and have a low survival rate. C57BL/6 wide-type (WT) mice were served as the control group.

Animal models

Mice (8 weeks old, Male) were anesthetized by intraperitoneal injection of 1% phenobarbitone (70 mg/kg body weight). Six of wild-type mice were used for sham, UUO or UIR performance respectively. Four or five of *Kcnk5*$^{flox/flox}$, *Kcnk5*$^{flox/flox}$/*Cdh16*^{Cre} mice were used as sham, UUO or UIR groups separately.

UUO model

The UUO model was prepared as described below. Briefly, the left ureter and kidney were exposed through a midline abdominal incision, and the ureter was isolated from the surrounding tissue and ligated with 5-0 silk. The left ureter was exposed but not ligated in Sham mice used as controls. Over the course of the study, six mice were included in each group. UUO mice were sacrificed 14 days after surgery.

UIR model

The UIR model was performed as described below. After midabdominal incision, the left renal pedicle was clamped for 30 min while mice were kept on a warming plate at 37°C. Mice were euthanized after 14 days to extract kidneys.

Human kidney samples

Kidney samples were obtained from patients with non (male, 21 years old), moderate (female, 38 years old) and severe (male, 52 years old) tubulointerstitium fibrosis recognized by skilled pathologists, depending on kidney biopsy findings with basal techniques, including light microscopy. Biopsy samples were with informed consent from the patients and in accordance with the Declaration of Helsinki.

Cell lines

Human immortalized proximal tubular epithelial cells, HK-2 cells originally obtained from ATCC, (CRL-2190). They were maintained at 37°C with 5% CO_2 in keratinocyte serum-free medium (Keratinocyte-SFM, Gibco Life Technologies), supplemented with epidermal growth factor (EGF; 5 ng/mL) and bovine pituitary extract (40 pg/mL).

Study approval

All animal experiments were approved by the Institutional Animal Care and Use Committee of Fudan University and adhered strictly to the National Institutes of Health Guide for the Care and Use of Laboratory

Animals. For the human studies, biopsy samples were obtained from renal biopsies at Zhongshan Hospital, Fudan University of China with informed consent from the patients and in accordance with the Declaration of Helsinki, approved by the Ethics Committee of Zhongshan Hospital, Fudan University (approval number: 20190506).

METHOD DETAILS

Methylated RNA immunoprecipitation sequencing (MeRIP-seq) and data analysis

MeRIP-seq was performed as described below. Briefly, purified mRNA from the kidney of UUO and Sham mice was chemically fragmented into 100-nucleotide-long fragments by incubation in 20-μL fragmentation buffer [10 mM Zn^{2+} and 10 mM Tris-HCl (pH 7.0)] at 94°C for 5 to 7 min. Size distribution of the fragmented mRNA was confirmed by agarose gel electrophoresis. Fragmented mRNA was immunoprecipitated with an anti-m^{6}A antibody (Cat#202003; Synaptic Systems, Goettingen, Germany), with some of the fragmented mRNA maintained kept as input. Input mRNA and m^{6}A-antibody-enriched mRNA were used for library construction using the KAPA stranded mRNA-seq kit (Cat#KK8421; Illumina, San Diego, CA, USA). Clustered libraries were then sequenced on an Illumina NovaSeq 6000 system using the NovaSeq 6000 S4 reagent kit (300 cycles; Illumina) according to manufacturer instructions. The raw reads were trimmed using Trimmomatic software and compared with the Ensemble reference genome using HISAT2 software.[50,51] Peaks in m^{6}A -RIP-enriched regions and differentially-methylated peaks (fold changes >1.5 and $p < 0.05$) between UUO and Sham mice were determined by MACS software.[52] These differential peaks were annotated using the latest Ensemble database. Sequence motifs are one of the basic functional units of molecular evolution, and we used MEME-ChIP to find motifs among the m^{6}A peak sequences.[53] MeRIP-seq data were uploaded to DRYAD (https://doi.org/10.5061/dryad.r2280gbbz).

MeRIP-quantitative (q)PCR

Real-time qPCR (qPCR) was performed to assess the relative abundance of *KCNK5* mRNA in m^{6}A-antibody immunoprecipitated samples and input samples between meclofenamic acid (MA)-, transforming growth factor-β (TGF-β)-, MA+TGF-β-, and vehicle-treated HK-2 cells. total RNA was extracted using Trizol reagent (Invitrogen, Carlsbad, CA, USA). After saving 50 ng of the total RNA as input, the remaining RNA (2 μg) was used for m^{6}A-IP with anti-m^{6}A (Synaptic Systems) in 500 μL of IP buffer [150 mM NaCl, 0.1% NP-40, 10 mM Tris (pH 7.4), and 100 U RNase inhibitor] to obtain the m^{6}A-pulldown portion. m^{6}A RNA was immunoprecipitated with Dynabeads Protein A (Thermo Fisher Scientific, Waltham, MA, USA) and eluted twice with elution buffer [5 mM Tris-HCL (pH 7.5), 1 mM EDTA (pH 8.0), 0.05% SDS, and 20 mg/mL Proteinase K]. m^{6}A-IP RNA was recovered by ethanol precipitation, after which 2 ng of total RNA and m^{6}A-IP RNA were used as templates for qRT-PCR, as described. The *hypoxanthine phosphoribosyltransferase 1* (*Hprt1*) gene served as an internal control, because *Hprt1* mRNA showed no m^{6}A peaks from m^{6}A-profiling data.[48]

Histopathological examinations and immunofluorescence staining

Kidney paraffin sections and frozen sections

Kidney paraffin sections and frozen sections were prepared as described below. Kidney tissues were fixed in 10% formalin, embedded in paraffin or OCT, and cut into 5-μm sections. For pathologic staining, paraffin sections or renal biopsy kidney tissues from patients with tubulointerstitial fibrosis were stained with a Masson's trichrome staining kit (Solarbio@LIFE SCIENCE, Beijing, China). Renal fibrosis scores were evaluated by light microscopy by a pathologist blinded to the origin of the preparations and determined using a scoring system. The degree of fibrosis was quantified with the photoshop image program by adjusting the threshold of color settings. The image analysis program was configured to detect areas of blue-stained collagen within each renal transverse section stained by Masson's trichrome. By reverse selection of the background, the software calculated the area of renal parenchyma. The fractional area of collagen was expressed as a percentage of the total area of renal parenchyma.

Immunofluorescence staining

To investigate TASK-2 distribution in different segments of renal tubules, we performed immunofluorescence double staining of paraffin sections. Briefly, after incubation with 0.3% bovine serum albumin, the slices were incubated with mixed primary antibodies: goat anti-TASK-2 (1:50) plus rabbit anti-aquaporin 1 (AQP1; 1:200) or rabbit anti-Tamm–Horsfall protein (THP; 1:100) or rabbit anti-NaCl co-transporter (NCC; 1:100) or rabbit anti-aquaporin 2 (AQP2; 1:200) or mouse anti-FTO (1:100). To evaluate the cell cycle, frozen

sections were reacted with a mouse antibody targeting phosphorylated histone H3 (Ser10) (pH3; 1:100), rabbit anti-Ki67 (1:100) and Streptavidin anti-LTL (1:200). To measure interstitial fibrosis, frozen sections were incubated with rabbit anti-α-smooth muscle actin (SMA; 1:100) and mouse anti-E-cadherin (1:100). After washing with phosphate-buffered saline (PBS), the immunoreaction was detected by Alexa Fluor 594-conjugated donkey anti-goat IgG (1:200; Thermo Fisher Scientific), Alexa Fluor 488-conjugated donkey anti-rabbit IgG (1:200; Thermo Fisher Scientific), Alexa Fluor 594-conjugated donkey anti-rabbit IgG (1:200; Thermo Fisher Scientific), Alexa Fluor 488-conjugated donkey anti-mouse IgG (1:200; Thermo Fisher Scientific) and Alexa Fluor 647-conjugated Streptavidin (1:200; YEASEN, Shanghai, China) by confocal microscopy.

Masson's trichrome staining

For pathologic staining of human kidney sections, paraffin sections were stained with a Masson's trichrome staining kit (Solarbio@LIFE SCIENCE, Beijing, China). To investigate TASK-2 distribution in renal proximal tubules, we performed immunofluorescence double staining of TASK-2 and LTL in paraffin sections, as described above. The study related to human kidney autopsy specimens was conducted in accordance with the Declaration of Helsinki, 2013, and approved by the Ethics Committee of Zhongshan School, Fudan University.

Cell treatments

Human proximal tubular cells (HK-2 cells; ATCC, Manassas, VA, USA) were cultured in DMEM/F12 medium (Keygen, Nanjing, China) containing 10% feta; bovine serum (FBS), 1 g/L insulin, 0.55 g/L transferrin, 0.67 mg/L selenium, 2 mM glutamine, 100 U/mL penicillin, and 100 mg/mL streptomycin in a humidified atmosphere with 5% CO_2 at 37°C until confluence. To induce fibrosis *in vitro*, HK-2 cells were treated with different concentration of TGF-β (2, 5, 10,15 ng/mL; Abcam, Cambridge, UK) for 24 h in FBS-free medium. Extracellular alkalization was induced by exposing culture medium to 30 mM $NaHCO_3$ (with appropriate amounts of NaCl used as a control). To block TASK-2, cells were pretreated with quinidine (20, 40, 60, 80, or 100 μM), clofilium (100 μM) or vehicle for 30 min prior to TGF-β treatment. To inhibit FTO activity, cells were pretreated with MA (20, 40, 60, 80, and 100 μM) or vehicle 30 min prior to TGF-β treatment. For RNA silencing, *KCNK5* or *FTO* small-interfering (si)RNA (Genepharma, Shanghai, China) was transfected into cells using Lipofectamine 3000 (Invitrogen) according to manufacturer instructions. The transfection was completed within ~6 h to ~8 h, followed by exposure of the cells to normal media. For TASK-2 overexpression, *KCNK5* plasmid (ZORIN, Shanghai, China) was transfected into cells for 4~6 h using Lipofectamine 3000 (Invitrogen) according to manufacturer instructions. ZV302(CMV-copGFP-T2A-puro-H1-MCS-3XFlag) serves as control. Then it was replaced with normal media for another 24 h followed by TGF-β treatment as described. The human *KCNK5*, *FTO* siRNA and *KCNK5* plasmid sequences are given in Table S2. Quinidine, clofilium and MA (CSNpharm, Shanghai, China) were dissolved and diluted separately in DMSO to a 20-mM stock solution.

Western blotting

Proteins were isolated from homogenized frozen kidneys or cell lysate homogenates, and western blot was performed. Briefly, samples (40 μg protein/lane) were loaded and separated on a sodium dodecyl sulfate-polyacrylamide gel and transferred to a polyvinylidene fluoride membrane, which was blocked with 5% nonfat milk and incubated with primary antibodies against TASK-2 (1:200), FTO (1:1000), AlkB homolog 5 (ALBKH-5; 1:1000), METTL3 (1:1000), METTL5 (1:1000), METTL14 (1:1000), METTL15 (1:1000), METTL7 (1:1000), E-cadherin (1:1000), fibronectin (FN)-1 (1:1000), α-SMA (1:1000), and glyceraldehyde 3-phosphate dehydrogenase (GAPDH; 1:5000) overnight at 4°C. Samples were then incubated with horseradish peroxidase (HRP)-conjugated secondary antibodies and developed using chemiluminescent HRP substrate. Results were normalized to GAPDH expression.

Real-time quantitative PCR

Total RNA was extracted with Trizol reagent (Invitrogen), and first-strand cDNA was then synthesized by reverse transcription using oligo (dT) and Superscript II (TOYOBO, Osaka, Japan) according to manufacturer instructions. PCR reactions were performed using SYBR-green PCR master mix (TOYOBO). Target gene and their primer sequences are shown in Table S3. Relative levels of mRNA expression were normalized to *Gapdh* expression for mouse samples.

Wound healing

For wound-healing assay, cells were seeded and cultured until 90% confluence. Cells were then scratched using a sterile pipette tip and washed twice with PBS. Cells were treated as indicated in FBS-free medium for 24 h. Cell-migration distances into the scratched area from the baseline to the 24-h time point were measured under a microscope.

CCK-8 assay

Cells (5000 cells/well) were plated onto 96-well culture plates, and after treatment, cell proliferation was detected by CCK-8 assay (Dojindo, Kumamoto, Japan). Optical density was measured by a microplate reader at 450 nm.

Intracellular pH and potassium measurement

Intracellular pH and K^+ measurement using a carbon dot-based inorganic–organic pH-sensitive probe (CDs@FITC) and an aptamer-based FRET nanoflare K^+ probe (AuNPs@aptamer), respectively.[54,55] HK-2 cells were treated, as described, and then incubated at 37°C with the pH probe for 1 h or the K^+ probe for 4 h. The cells were then washed with PBS or saline to remove redundant probes and incubated in calibrating solutions at 37°C for 15 min, followed by measurement by flow cytometry. The pH-dependent fluorescence was observed after excitation at 488 nm, and the fluorescence signal was acquired in the range of 500 nm to 560 nm (first column; FITC) and 655 nm to 735 nm (second column, reference dye). K^+-dependent fluorescence was excited at 488 nm, and the fluorescence signal was acquired in the range of 500 nm to 560 nm (first column; FAM) and 548 nm to 600 nm (second column; TAMRA). Standard curves were plotted by the ratio of mean fluorescence intensities of two columns (FITC/reference dye or TAMRA/FAM) versus the pH or K^+ concentrations of the calibrating solutions, respectively. The solution used for intracellular pH measurements included the following (mM): 30 NaCl, 120 KCl, 1 $CaCl_2$, 0.5 $MgSO_4$, 1 NaH_2PO_4, 5 D-glucose, and 20 HEPES (pH 7.4). The calibrating solutions used for the pH standard curve comprised the measurement solution adjusted with HCl or NaOH to various pH levels (6.9, 7.0, 7.1, 7.2, 7.3, 7.4, 7.5, and 7.6) with 10 μM nigericin (Aladdin Bio-Chem Technology Co., LTD., Shanghai, China). The solution for intracellular K^+ measurement included the following (mM): 145 NaCl, 5 KCl, 1.8 $CaCl_2$, 1 $MgSO_4$, 1 NaH_2PO_4, 10 D-glucose, and 32.2 HEPES adjusted with NaOH to pH 7.4. The calibrating solutions used for the K^+ standard curve comprised the measurement solution but with different Na^+ concentrations (125, 100, 75, 50, 25, and 0 mM) and K^+ concentration (75, 100, 125, 150, 175, and 200 mM). The sum concentration of NaCl and KCl was 200 mM and with the addition of 1 μM valinomycin (Aladdin Bio-Chem Technology Co., LTD.) and 10 μM nigericin (Aladdin Bio-Chem Technology Co., LTD.).

Propidium iodide (PI) staining

PI staining was performed to detect cell cycle progression. After treatment, HK-2 cells were harvested at ~80% confluence for further fixation and staining using a cell cycle detection kit (Keygen) according to manufacturer instructions. Flow cytometry was used to detect cell cycle phase, and the percentages of cells in different phases was analyzed according to their DNA content.

QUANTIFICATION AND STATISTICAL ANALYSIS

Statistical analysis was performed with the GraphPad Prism software version 8.2.0 for Windows (GraphPad Software, San Diego, CA). Data are presented as the mean ± standard deviation. For comparison between two groups, two-tailed unpaired *t* tests were used. For multiple comparisons, one-way ANOVA or Two-way ANOVA followed by the Tukey post-hoc was applied. All comparisons were two-tailed, and a $p < 0.05$ was considered significant. All statistical details of experiments can be found in the figure legends.